RMP
REGIONAL MONITORING
PROGRAM FOR WATER QUALITY
IN SAN FRANCISCO BAY

sfei.org/rmp

Water and Suspended-Sediment Flux Measurements at the Golden Gate, 2016-2017

Prepared by

Maureen Downing-Kunz, U.S. Geological Survey

David Schoellhamer, U.S. Geological Survey

Paul Work, U.S. Geological Survey

CONTRIBUTION NO. 856 / DECEMBER 2017

SAN FRANCISCO ESTUARY INSTITUTE • CLEAN WATER PROGRAM/RMP • 4911 CENTRAL AVE., RICHMOND, CA • WWW.SFEI.ORG

Water and Suspended-Sediment Flux Measurements at the Golden Gate, 2016-2017

Maureen Downing-Kunz

David Schoellhamer

Paul Work

United States Geological Survey
California Water Science Center
Placer Hall, 6000 J Street, Sacramento, CA 95819

In partnership with the
Regional Monitoring Program for Water Quality in San Francisco Bay

29 December 2017

SFEI Document Number: 856

This work was partially funded as a result of settlement of
San Francisco Bay Water Board enforcement actions

Acknowledgments

Funding for this work was provided by the San Francisco Bay Water Quality Improvement Fund through EPA Region 9, the San Francisco Estuary Partnership, and the Regional Monitoring Program for Water Quality in San Francisco Bay. This work was partially funded as a result of settlement of San Francisco Bay Water Board enforcement actions. The authors wish to acknowledge members of the Estuarine Sediment Transport Project and others at the USGS for their support in data collection, including Paul Buchanan, Gwen Davies, Brian Downing, Darin Einhell, Daniel Livsey, Scott Nagel, and Kurt Weidich, as well as Mark Stacey of UC-Berkeley and David Stevens of Utah State University.

Executive summary

Sediment is an important resource for San Francisco Bay (SFB), in the context of restoration projects, dredging operations, ecosystem health, and contaminant transport and fate. Understanding the transport and fate of sediment in SFB is important to ecosystem researchers and managers. Previous studies have shown that sediment exchange at the estuary-ocean boundary of SFB (Golden Gate inlet) is the most poorly understood element of the SFB sediment budget, owing to logistical challenges that inhibit routine field observations, and the fact that net flux is a small fraction of the instantaneous peak values experienced on a daily basis. Improved understanding of sediment exchange at the estuary-ocean boundary of SFB is essential to updating SFB-wide sediment budgets, which account for sources, sinks, and storage of sediment (and sediment-associated contaminants).

In this study, field observations of water and suspended-sediment fluxes at the Golden Gate were made over one ebb tide and one flood tide on three occasions:

1) 21-22 March 2016, following a large storm event that triggered the first flow into Yolo Bypass flood control structure since 2011
2) 23 June of 2016, during a period of low freshwater inflow;
3) 27-28 February 2017, following several large storms of the wettest winter in northern California in recorded history.

On each occasion, flux of water and suspended sediment were estimated using data from a boat-mounted acoustic Doppler current profiler. This instrument provided high-resolution velocity and acoustic backscatter (ABS) data at a cross-section ("transect") near the estuary-ocean boundary, approximately 1 km landward (east) of the Golden Gate Bridge. Discrete water samples collected *in situ* were analyzed for suspended-sediment concentration (SSC) and related to ABS to allow quantification of sediment concentrations and fluxes.

During the March 2016 field campaign, peak discharge from the Central Valley watershed (estimated from DAYFLOW model) was 4,100 m^3/s and maximum discharge observed at the transect reached 130,000 m^3/s during ebb tide; peak suspended-sediment flux at the transect was nearly equivalent for ebb and flood tides (2100 kg/s). Observed transect-average SSC values (mean: 21 mg/L; range: 17-27 mg/L; n=18) were lower than expected based on upstream

conditions—a network of five SSC monitoring stations extending 5-80 km upstream demonstrated a watershed-sourced sediment pulse (SSC reaching 200 mg/L) moved downstream to San Pablo Bay, an observation corroborated qualitatively by concurrent satellite imagery. This observation, combined with lower SSC toward the Golden Gate, suggests the sediment pulse was trapped within SFB.

During the June 2016 field campaign, discharge from the Central Valley watershed was small (200 m^3/s) and below average for the date (1956-2015 average for 23 June: 350 m^3/s), but typical for late-summer conditions (1956-2015 average for 13 August: 180 m^3/s). Peak discharge and suspended-sediment flux at the transect were 120,000 m^3/s on the ebb tide and 2100 kg/s on the flood tide, respectively. Transect-average SSC values during June 2016 (mean: 26 mg/L; range: 19-35 mg/L; *n*=9) were similar to those observed in March 2016, as was the peak suspended-sediment flux; these observations further suggest the March 2016 storm was not sufficient to force the sediment plume out of SFB.

During the January 2017 field campaign, peak discharge from the Central Valley watershed (10,700 m^3/s) was 2.6 times larger than that occurring in 2016. Peak discharge observed at the transect was 120,000 m^3/s, equivalent to the peak observed in June 2016, demonstrating that the volume of water delivered from the Central Valley watershed is small compared to the tidal prism of San Francisco Bay. Peak suspended-sediment flux at the transect for ebb and flood tides was 3800 kg/s and 5800 kg/s, respectively, indicating more sediment transported landward (flood-tide directed) than seaward (ebb-tide directed). Observed transect-average SSC values (mean: 47 mg/L; range: 38-64 mg/L; *n*=32) demonstrated that more sediment was in suspension near the estuary-ocean boundary during January 2017 than during the two previous field campaigns. Inspection of up-estuary SSC showed a magnitude of watershed-sourced sediment pulse similar to March 2016 (~200 mg/L), but much higher SSC at the seaward end of San Pablo Bay (~600 mg/L). Analysis of up-estuary salinity, demonstrating freshwater throughout the water column at the landward edge of San Pablo Bay, offered a plausible explanation of the formation of an estuarine turbidity maximum (ETM) in San Pablo Bay, which would cause trapping of sediment. Thus we suspect trapping of watershed sediment discharge occurred in San Pablo Bay for the events in March 2016 and February 2017.

Application of a previously developed surrogate relationship for Golden Gate sediment flux based on field measurements at Alcatraz Island was unsuccessful due to methodological problems with the previous study. However, field observations suggest the general approach is reasonable and promising, but further work is required. Development of a numerical model is recommended to better understand sediment flux at the ocean boundary of SFB over longer time scales.

Introduction

Sediment is an important resource for San Francisco Bay (SFB, Fig. 1), in the context of restoration projects, dredging operations, ecosystem health, and contaminant transport and fate. Understanding the transport and fate of sediment in SFB is important to ecosystem researchers and managers. For SFB, sources of sediment include the Central Valley watershed via the Sacramento-San Joaquin Rivers Delta (Delta), local tributaries adjacent to SFB, sand entering from the Pacific Ocean along the bottom at the estuary-ocean boundary, and inflow of suspended sediment from the ocean during flood tides; sinks (or losses) of sediment include outflow of sediment suspended in the water column to the Pacific Ocean, dredging with disposal outside of SFB, commercial sand mining, and deposition in wetlands (Schoellhamer et al., 2005).

Previous studies (*e.g.,* Schoellhamer et al., 2005; Erikson et al., 2013) have shown sediment outflow at the estuary-ocean boundary, the Golden Gate inlet (Fig. 2), to be the most poorly understood element of the SFB sediment budget. Sediment outflow at the Golden Gate following storms has been observed via remote sensing (Ruhl et al., 2001), but existing field observations of sediment exchange (inflow and outflow) are relatively sparse: Teeter et al. (1996) conducted field measurements during dry weather conditions in 1988 and 1992; and Erikson et al. (2013) conducted field measurements during the wet season of 2008. The paucity of field observations of sediment exchange at the Golden Gate inlet are attributed to difficult conditions arising from its physical characteristics: the inlet width exceeds 1.5 km, 100 m in depth, and experiences a tidal range of nearly 2 m, giving rise to tidal currents in excess of 2 m/s. Additionally, the tidal exchange of water at the inlet far exceeds the net or residual flow to the ocean, such that the determination of net flow requires careful averaging measurements of very large reversing flows.

In this study, we sought to augment existing field observations of sediment exchange at the Golden Gate with measurements on three different occasions:

1) 21-22 March 2016, following a large storm event that triggered the first flow into Yolo Bypass flood control structure since 2011
2) 23 June of 2016, during a period of low freshwater inflow;
3) 27-28 February 2017, following several large storms of the wettest winter in recorded history of northern California.

Erikson et al. (2013) integrated field measurements and numerical modeling to develop an empirical relationship using suspended-sediment concentration measured at Alcatraz Island (USGS station ID 374938122251801) as a surrogate to quantify suspended–sediment flux and estimate sediment exchange at the Golden Gate. We attempted to apply this surrogate method to estimate sediment exchange at the Golden Gate. The approach defined in Erikson et al. (2013), however, makes use of the product of the tidally averaged SSC and the tidally averaged velocity, with the latter computed from harmonic constituents. With this approach, the tidally averaged velocity is zero and therefore the tidally averaged sediment flux would be zero. While the approach was sound the method was not useable, so further refinement of this methodology is required to predict Golden Gate flux. Additional numerical modeling, which was not included in the project that led to this report, will be required.

Methods

Acoustic measurements of water discharge and suspended-sediment concentration (SSC) at a cross section at the Golden Gate (Fig. 2) were used to estimate suspended-sediment flux over a range of tidal and hydrologic conditions. Water samples collected *in situ* were used to relate acoustic backscatter to SSC.

Boat-based measurements of water velocity and acoustic backscatter

At a defined cross-section ("transect") approximately 1 km landward of the Golden Gate inlet (dashed line in Fig. 2), three-dimensional velocity and echo intensity data were collected using a boat-mounted acoustic Doppler current profiler (ADCP, Workhorse 600 kHz, Teledyne RD Instruments, San Diego, CA; the use of firm, trade, and brand names is for identification purposes only and does not constitute endorsement by the USGS). The ADCP was deployed in

down-looking mode from San Francisco State University's 38-foot *R/V Questuary* during the March 2016 field trip (Fig. 3), from the USGS' 26-foot *R/V Dinehart* in June 2016 (Fig. 4), and again from the *R/V Questuary* in February 2017.

The ADCP contains four transducers that transmit packets of acoustic energy into the water column. A fraction of this energy is returned to each transducer by scattering from particles in the water column. The frequency shift between transmitted and returned signals allows for computation of along-beam velocities for each of the four transducers. Knowing the orientation of these beams and the pitch, roll, and heading of the instrument, East-West, North-South, and up-down velocity components can be computed. Range-gating of the acoustic return signal allows vertical resolution of velocities in fixed depth bins (in this study: 50 cm in vertical extent). In addition to velocity, the ADCP also reports echo intensity, a measure of the power of the return signal. Echo intensity (in counts) from each of the four beams was converted to sediment-corrected acoustic backscatter (ABS, in decibels, dB) by accounting for sound absorption, beam spreading, and sediment attenuation (Landers et al., 2016), yielding a four-beam average of ABS for each depth bin. Teledyne RD Instruments' WinRiver II software was used to record velocity, depth, echo intensity, and ABS data while underway.

The primary outputs from the ADCP utilized in this study were vertical profiles of velocity and ABS from known locations in horizontal space (based on ADCP bottom track and/or GPS data) at 1 Hz; from these data, the spatial distribution of water velocity and ABS were estimated for each transect.. Because the ADCP is deployed just beneath the surface of the water, the near-surface region (0-1 m from surface) was not sampled. Due to irregularities in the bed surface, the ADCP ignores signal return and does not compute velocity nor ABS in the near-bed region (6% of the distance between the transducers and the bed plus one depth bin (Teledyne RD Instruments, 2016), or 5-10 m from bed); however the total depth is observed. In addition, the boat cannot access the entire width of the transect due to shallow regions along both shores. The result is that velocity and ABS are not measured for about 10% of the cross section; occasional communication errors between the ADCP and computer sometimes led to additional missing data. Missing velocity data near the surface and bed were filled using hydraulic theory (Simpson and Oltmann, 1990; Chen, 1991) while missing velocity (and ABS) data from the water column were filled via linear interpolation in the horizontal direction, as long as the gaps had lengths less

than 50 m and were bounded by good data (*i.e.*, no extrapolation). Water velocity normal to the boat track was computed as follows:

$$V_{normal} = V * \sin(\pi/180*(\Theta\text{-}heading)) \quad \textit{(Eq. 1)}$$

where V_{normal} = water velocity normal to boat track in m/s;

V = ADCP velocity magnitude in m/s, linearly interpolated as needed;

Θ = velocity vector direction in degrees; and

heading = ADCP heading in degrees.

Due to the large width of the transect (3.2 km), each transect duration was 20-30 min. The transect path was deliberately chosen to avoid the very deepest portions of the Golden Gate while still capturing the entire flow (Fig. 2). Had a transect along a deeper region been chosen, the range of the ADCP would have been exceeded and flow would not have been measured. A lower frequency ADCP could have been used to increase the vertical range for velocity measurements, but this would have decreased vertical resolution, and also lead to reduced sensitivity for estimating sediment concentrations in the water column.

Relation of acoustic backscatter to suspended-sediment concentration

Sediment in the water column both reflects and dissipates the energy of sound propagating through the water and is a major component of acoustic backscatter, which has been used as a proxy for SSC (Gartner, 2004; Wall et al., 2006; Landers et al., 2016). To develop the proxy, concurrent observations of sediment-corrected acoustic backscatter and *in situ* water samples analyzed for SSC were collected. Water samples were also analyzed for mass fractions of fine- and sand-sized particles (diameter less than or greater than 63 μm, respectively). Because the acoustic response of sediment is dependent on the instrument frequency, the same frequency ADCP was used for all field measurements, and water samples were collected during each field campaign. Note that for calibration purposes, it is not necessary to obtain water samples from the same transect where the velocity data are being collected, nor at the same time, but samples must be representative of the environment of interest, and it is desirable to span a wide range of conditions. The primary assumption is that when and where data are collected for calibration purposes, the characteristics of the suspended sediment (size, size distribution, shape, density) mirror those of the site being surveyed. In this study, the term acoustic backscatter, ABS, is used

to indicate sediment-corrected backscatter (as described above), which can be used as a proxy for SSC (Landers et al., 2016).

The methodology for collection of suspended-sediment samples differed between the three field campaigns. In March 2016, a boat-mounted, depth-integrating, isokinetic sampler (Model D-96, Federal Interagency Sedimentation Project, 2001), along with a horizontally positioned Van Dorn-style sampler, were used. The former is lowered gradually and steadily through the water column, while open, and thus yields a depth-integrated estimate of suspended-sediment concentration. The Van Dorn-style sampler is a plastic tube with rubber stoppers at each end which are held open until triggered; the sampler is lowered to the depth of interest and snapped closed, thus yielding an instantaneous estimate of concentration at a point. Two boats were used, one to acquire velocity data and the other to obtain water samples for SSC.

During the June 2016 and February 2017 field campaigns, a boat-mounted, point-integrating, isokinetic sampler (P-61, Edwards and Glysson, 1999) was used (Fig. 4). This sampler has a solenoid to allow it to be opened for a specified duration at a depth of interest, providing a time-integrated sample at a given depth. For these field campaigns, one boat was used; the ADCP and P-61 were deployed from the *R/V Dinehart* to obtain concurrent ABS measurements and water samples. Additionally, point-instantaneous water samples were collected at the Golden Gate from the *R/V Questuary* to quantify SSC and percent fine-sized particles during transecting.

To develop a calibration curve relating ABS to SSC, ordinary least squares regression analysis was used, with ABS as the explanatory variable for log-transformed SSC, as follows:

$$log_{10}(SSC) = b_0 + b_1 * ABS \qquad (Eq.\ 2)$$

where SSC = suspended-sediment concentration in mg/L;

ABS = sediment-corrected acoustic backscatter in dB;

b_0 = y-intercept; and

b_1 = slope.

To predict SSC, this log-transformed linear model is retransformed as:

$$SSC = 10^{(b_0 + b_1 * ABS)} * BCF \qquad (Eq.\ 3)$$

where SSC = suspended-sediment concentration in mg/L;

ABS = sediment-corrected acoustic backscatter in dB;

b_0 = y-intercept;

b_1 = slope; and

BCF = bias correction factor to account for retransformation bias (Rasmussen et al., 2009).

For depth-integrated (D-96) samples, ABS used in the regression was computed as the average value of the four beams over the depth sampled (all bins within the depth sampled) and over the entire time the D-96 was in the water (generally ~2 min). For point (Van Dorn) samples, ABS was computed as the mean of the four beams over the depth bin nearest the sample depth for 0.5 min surrounding the sample. For point-integrated (P-61) samples, ABS was computed as the mean of the four beams over the depth bin nearest the sample depth over the time the sampler nozzle was open (sample duration range: 0.75-1.5 min). For point and point-integrated samples, the four-beam average ABS for the four depth bins surrounding the bin nearest the sample depth were inspected to ensure uniform ABS across depth and over time. Two separate calibration curves were developed for 2016 and 2017 field campaigns, respectively.

Computation of water flux and suspended-sediment flux

For each complete ADCP transect, flux of water and suspended sediment were calculated. Water flux (discharge) was calculated by integrating the computed track-normal velocity (V_{normal}, Eq. 1) over the flow area. SSC in each depth bin was computed from the four-beam average ABS according to Equation 3. Suspended-sediment flux was then computed as the product of SSC and V_{normal} in each depth bin, integrated over the flow area to obtain total suspended-sediment flux for each transect in terms of mass per unit time (Tables 3-5). Transect-average SSC was computed as the average SSC over all depth bins for each transect. Horizontal interpolation was employed to fill gaps in the velocity and ABS records, as needed, where gaps spanned less than 50 m horizontally. Larger gaps, which were infrequent, were not included in area and flux computations. Communication problems in the two 2016 campaigns led to many dropouts in the GPS log, but bottom track data from the ADCP allowed computation of fluxes. Temporal averaging (which would also imply spatial averaging, since the measuring instrument is moving)

was not used, but the horizontal integration involved in computing fluxes of water and sediment should remove much of the random error in the measured velocity and backscatter fields.

Ancillary data

Observed tidal stage data were sourced from San Francisco, CA (NOAA station ID 9414290). Tides at the Golden Gate are mixed semi-diurnal, with a maximum range of 1.8 m. Freshwater inflow to SFB was estimated as the freshwater flow out of the Delta, referred to as "Delta outflow". Daily estimates of Delta outflow were obtained from the DAYFLOW model (CDWR, 1986). Freshwater discharge into Yolo Bypass (USGS station ID 11453000), a flood control structure on the Sacramento River near Woodland, CA. Delta outflow and Yolo Bypass discharge were used as indicators for storm magnitude.

Salinity and suspended-sediment concentrations at up-estuary locations within SFB were obtained from continuous water-quality monitoring stations at Benicia Bridge (USGS station ID 11455780), Carquinez Bridge (salinity only; USGS station ID 11455820), Richmond Bridge (USGS station ID 375607122264701), and Alcatraz Island (USGS station ID 374938122251801) (Fig. 1). At these monitoring stations, data are collected at one or two depths every 15 min; provisional data are transmitted hourly and accessible via the National Water Information System website (http://waterdata.usgs.gov/nwis). More details are available in Buchanan et al. (2014). Timing of the wet season field campaign was determined in part by the SSC data from these up-estuary stations. Tidal filtering of salinity and SSC time series was performed using a low-pass Butterworth filter with a 30-hour stop period and a 40-hour pass period.

Results

Field campaigns

Field measurements were conducted on ebb and flood tides during wet and dry periods in 2016 (Fig. 5) and one extremely wet period in 2017 (Fig. 6); see Table 1 for a summary of the salient details of each field campaign. Spring tides were selected for field measurements because we expected higher likelihood of capturing watershed-sourced sediment plumes; during spring tides, tidal excursions are higher, which would transport watershed-sourced plumes closer to the ocean boundary, and tidal velocities are higher, which would increase vertical mixing (Simpson et al., 1990; Schoellhamer, 2002). In 2016, a Central Valley watershed-sourced sediment plume was

identified in satellite imagery on 16 Mar 2016 (Fig. 7), during a period of falling salinity and rising SSC at SFB stations (Figs. 5B-C). Delta outflow increased in early March 2016 and reached a peak value of 4100 m^3/s on 16 March 2016 (Fig. 5A; Table 1). Sacramento River flood waters spilled into the Yolo Bypass between 12 March 2016 and 22 March 2016, with peak flow of 2300 m^3/s on 15 March 2016 (Fig. 5A). Based on previous estimates of sediment plume travel time (Erikson et al., 2013) and predictions for spring tide, wet season sampling was conducted 21-22 March 2016 with the ebb tide sampled on 21 March and the flood tide sampled on 22 March (Fig. 8A). Dry season sampling was conducted for subsequent ebb and flood tides on 23 June 2016 (Fig. 8B) during a period of low freshwater inflow (Fig. 5A; Table 1).

Winter of 2017 was much wetter than that of 2016; precipitation indices for eight stations in the northern Sierra Nevada Mountains (within the watershed of Sacramento River) during January 2017 and February 2017 were 2.6 and 2.9 times higher, respectively, than the long-term monthly average (CDWR, http://cdec.water.ca.gov/prev_barcharts8SI.html, accessed 12/11/17), leading to several major northern California reservoirs reaching near-total storage capacity by 10 Feb 2017 (Reservoir Name: percentage of total reservoir capacity on 2/10/17: Shasta: 96%; Oroville: 100%; Don Pedro: 97%, CDWR, http://cdec.water.ca.gov/resapp/RescondMain, accessed 12/11/17). The magnitude of the peak freshwater inflow to SFB (as estimated by Delta outflow) was 2.6 times larger in 2017 compared to 2016 (Table 1 and Fig. 9). In 2017, Delta outflow increased sharply in early February to a peak value of 10,700 m^3/s on 11 Feb 2017, remaining above 8000 m^3/s during much of February until another round of storms and reservoir releases produced a secondary peak value of 9500 m^3/s on 22 Feb 2017 (Fig. 6A; Table 1). In response to the larger freshwater flows in 2017, near-bed salinity at SFB stations was lower in magnitude for a longer duration than 2016 (Figs. 5B & 6B). Tidally filtered near-bed salinity at Carquinez Bridge reached zero for nearly one month (9 Feb 2017 – 3 Mar 2017, 22 days, Fig. 6B), indicating the watershed-sourced freshwater plume extended into San Pablo Bay (Fig. 1). Sacramento River flood waters spilled into the Yolo Bypass between 9 Jan 2017 and 3 May 2017 (114 days), with peak inflow of 5500 m^3/s on 22 Feb 2017 (Fig. 6A). The spring tide following the two Delta outflow peaks during February was targeted, and 2017 wet season sampling was conducted 27-28 Feb 2017 for 17 consecutive hours, beginning on a flood tide with stage rising to higher high tide, followed by an ebb tide with stage falling to lower low tide, and ending slightly past the subsequent lower high tide (Fig. 8C).

Post-processing of ADCP output

To demonstrate the procedures for post-processing ADCP data, the transect from 21 March 2016, beginning at 13:07 PST (Table 3) is used as an example. Figure 10 shows a plan view of this transect based on GPS data. During the March 2016 field campaign, GPS communications were problematic, so bottom tracking – the ADCP's internal computation of speed and direction, based on acoustic data – was used for boat speed and elapsed distance estimates instead of GPS. For the June 2016 and February 2017 datasets, GPS communications were improved and GPS data were used to obtain boat speed and position data. The cross-section view of raw velocity magnitude for the above-mentioned example transect is shown in Figure 11A—additional communication errors between the ADCP and the computer led to occasional dropped acoustic pings, resulting in the vertical white stripes in the water column seen in the top plot. The result after interpolation to fill missing data is shown in Figure 11B, and the track-normal component of velocity (Eq. 1) in Figure 11C. This particular example required much more interpolation than was required with any of the 2017 transects. Note also that in this example transect, the flow direction is out of SFB (ebb-tide directed), with higher velocities in the central part of the transect, and flood-directed flow at the ends of the transect (Fig. 11C).

Relation of acoustic backscatter to suspended-sediment concentration

Two calibration datasets of concurrent ABS and SSC (from point-integrating sampler) were used to produce two calibration curves, one for 2016 measurements (March and June, Fig. 12) and one for 2017 measurements (February, Fig. 13). During the 2016 field campaigns, three water sampling methodologies (sampler type in parentheses) were attempted: depth-integrated (D-96); point-instantaneous (Van Dorn); and point-integrated (P-61). Ultimately, the point-integrated sampling method was deemed most suitable for this study. For the March 2016 field campaign, the point-instantaneous samples were excluded for two reasons: first, they are instantaneous values of SSC and thus cannot be integrated over time to relate to an average ABS value from the ADCP; second, the weight on the Van Dorn sampler was insufficient to maintain the sampler at a known depth for locations with high water velocity. The depth-integrated water samples from March were also excluded from the calibration because the observed ABS was generally not uniformly mixed over depth, and the larger sampling volume compared to the point-integrated samples led to a calibration dataset spanning a low range of ABS (Fig. 12), with a

maximum value that was lower than maximum observed ABS in the transects. Additionally, the deployment of ADCP and D-96 from separate vessels during March 2016 made co-location of sampling volumes for ABS and SSC data difficult.

To improve the calibration dataset by increasing the range of ABS and co-locating ABS with SSC, the point-integrating sampler (P-61) was used in the June 2016 field campaign. Given the patchy distribution of SSC in this environment, the smaller sampling volume of the point-integrating sampler allowed for more precise sampling within relatively small regions of elevated SSC. The effort to span a greater range of ABS was successful for the June 2016 calibration dataset (Fig. 12); because these two 2016 calibration datasets employed different sampling techniques, only one calibration dataset should be utilized (Landers et al., 2016), and the June 2016 dataset was deemed higher quality. To verify the suitability of applying the June 2016 regression to the March 2016 measurements, the two datasets were inspected and showed favorable comparison (Fig. 12 and Table 2). Thus, the June 2016 calibration dataset was used to define the relation between ABS and SSC (Fig. 12) for March 2016 and June 2016 measurements. For the 2017 field campaign, only the point-integrated sampling method was used (Table 2).

All regression models (Table 2) produced slopes (b_1, Eq. 2) that are positive as expected, and within the range of expected values based on previous studies (range 0.03-0.1, Landers et al., 2016). All BCF determined from model residuals were within the expected range of 1.01-1.1 (Rasmussen et al., 2009). To compute SSC in each depth bin of complete transects for all field campaigns, the regression models were applied to the ADCP data as follows: the model from June 2016 was applied to transects collected in both March 2016 and June 2016; and the model from February 2017 was applied to transects collected in February 2017. An example of SSC computation is shown in Figure 14. Note that while some instrument pings that do not result in a velocity estimate, because of insufficient correlation, backscatter values are still reported. So there was less need for interpolation with the backscatter data.

Laboratory analysis of water samples indicated fine-sized particles (diameter less than 63 µm) dominated all periods: in March 2016, fine-sized particles for all samples represented more than 80 percent of the total mass for associated samples (mean: 89.7; range: 79.7-95.1; *n*=19); in June 2016, fines represented more than 84 percent of the total mass for associated samples (mean:

90.6; range: 83.6-97.2; *n*=16); and in February 2017, fines represented more than 48 percent of the total mass for associated samples (mean: 90.7; range 48.1-100.0; *n*=19).

Calculated flux of water and suspended sediment

During the March 2016 field campaign (Table 3 and Fig. 15), observed peak water flux magnitude occurred on the ebb tide (1.3e5 m^3/s, start time 13:43 PST on 3/21/16) approximately one hour before observed peak suspended-sediment flux magnitude was observed (2100 kg/s or 1.3e5 kg/min, start time 14:50 PST on 3/21/16). On the flood tide, peak flux of water and sediment were concurrent; although the magnitude of observed peak water flux (1.0e5 m^3/s, start time 08:46 PST of 3/22/16) was 20% smaller than that on the 3/21/16 ebb tide, the magnitude of peak sediment flux (2100 kg/s or 1.2e5 kg/min, start time 08:46 PST of 3/22/16) was only 2% smaller than that on the 3/21/16 ebb tide. Note that the difference between observed peak water flux for ebb and flood tides (2.1e4 m^3/s) does not indicate that the net outflow for the day was this high; it instead reveals the sum of the net outflow and the inequality of the semi-diurnal tides. During the March 2016 field campaign, observed transect-average SSC reached a maximum of 27.0 mg/L on the flood tide (start time 09:21 PST on 3/22/16, Table 3); the mean SSC for all transects from March 2016 was 21.0 mg/L (*n*=18).

During the June 2016 field campaign (Table 4 and Fig. 16), observed peak water flux magnitudes on ebb (1.2e5 m^3/s, start time 06:27 PST on 6/23/16) and flood (1.1e5 m^3/s, start time 12:53 PST on 6/23/16) tides were nearly equal (5% difference). Comparing the timing of observed peak suspended-sediment flux magnitude to that for observed peak water flux for ebb and flood tides, the peaks on ebb tide (1600 kg/s or 1.0e5 kg/min, start time 06:48 PST on 6/23/16) were approximately concurrent, while on flood tide (2100 kg/s or 1.3e5 kg/min, start time 10:53 PST on 6/23/16) they were not. The peak suspended-sediment flux on the 6/23/16 flood tide (-2100 kg/s, Table 4) was similar in magnitude to that observed during the 3/21/16 ebb tide (2100 kg/s, Table 3), despite occurring during the dry season. During the June 2016 dry period observations, observed transect-average SSC reached a maximum of 34.8 mg/L on the flood tide (start time 11:52 PST on 6/23/16, Table 4); the mean SSC for all transects from June 2016 was 26.0 mg/L (*n*=9).

The February 2017 field campaign took place during what eventually proved to be the wettest winter in northern California in recorded history (CDWR, http://cdec.water.ca.gov/cgi-progs/products/PLOT_ESI.2017.pdf, accessed 12/11/17). During the February 2017 measurements (Table 5 and Fig. 17), observed peak water flux magnitude on the ebb tide (1.2e5 m^3/s, start time 16:29 PST on 2/27/17) was 9% higher than that for flood tide (1.1e5 m^3/s, start time 22:30 PST on 2/27/17). However, the observed peak suspended-sediment flux magnitude on the ebb tide (3800 kg/s or 2.3e5 kg/min, start time 14:55 PST on 2/27/17) was 34% lower than that for flood tide (5800 kg/s or 3.5e5 kg/min, start time 22:59 PST on 2/27/17). The timing of the peak flux magnitudes for water and suspended sediment were not concurrent but nearly so; on the ebb tide peak sediment flux preceded peak water flux by about 0.5 h, while on the flood tide peak sediment flux lagged peak water flux by about 0.5 h (Table 5). During the February 2017 wet period observations, observed transect-average SSC reached a maximum of 63.9 mg/L on the flood tide (start time 22:59 PST on 2/27/17, Fig. 17); the mean SSC for all transects from February 2017 was 47.1 mg/L (n=32).

The 2017 measurements spanned enough time to capture one complete ebb tide (12:59-19:26 PST 2/27/17, Table 5) and one complete flood tide (19:33 PST 2/27/17-01:31 PST 2/28/17, Table 5), and the dataset also featured the best quality (fewest communications dropouts and thus least interpolation). The duration of the ebb (6.5 h) was slightly longer than that for the flood (6.0 h), in part because of the large freshwater outflow from the watershed. Net volumetric water flux through the cross section of the transect for each tide, computed by integrating water flux over the ebb and flood phases of the tide separately, was 24% greater on ebb tide (1.7e9 m^3) than on flood tide (1.3e9 m^3), in part due to the longer duration and greater peak water flux magnitude of ebb tide. However, net mass of suspended-sediment transported through the cross section of the transect, computed by integrating suspended-sediment flux over the ebb and flood phases of the tide separately, was 20% greater on flood tide (7.0e4 metric tons) than on ebb tide (5.5e4 metric tons). Despite the longer duration and greater peak water discharge of the ebb tide, giving rise to net seaward export of water, more sediment was transported landward on the flood tide, in part due to greater SSC throughout the water column on the flood tide.

The stated accuracy of the velocity measured by the ADCP used in this study is 0.3% of measured magnitude + 0.3 cm/s. Observed peak flows corresponded to cross-sectionally

averaged velocities close to 1 m/s. The rated errors would thus be 0.6 cm/s, which, if expressed as a flux, represents approximately 800 m^3/s, or about 0.6% of the measured water flux. Actual errors in water flux are likely larger than this, because this is only the ADCP error and does not include the boat velocity vector that is also used, but the total error should be less than the observed difference between ebb and flood flows. Errors in the computed sediment flux were not quantified here, but previous studies (Ganju et al., 2006; McKee et al., 2006; Downing-Kunz and Schoellhamer, 2013) suggest values near 30% are likely, much larger than those for water flux.

Discussion

Comparison of 2016 and 2017 field campaigns

During this study, a unique opportunity arose to conduct field observations of suspended-sediment flux at the estuary-ocean boundary following major watershed runoff in 2016 and again in 2017, as well as during dry season conditions. Daily Delta outflow during 2016 was generally lower than the long-term mean, except for the March 2016 storm (Fig. 9). In contrast, daily Delta outflow during 2017 was generally higher than the long-term mean, with an annual peak that was 2.6 times larger than that of 2016 (Fig. 9). Despite the higher flows in 2017, peak observed water flux at the Golden Gate transect was highest during March 2016, demonstrating that tidal forcing dominates the discharge signal at the estuary-ocean boundary of San Francisco Bay. The peak inflow from the Delta that was observed in WY2016 (4100 m^3/s, Figs. 5A & 9) is only 3% of the observed peak outflow at the Golden Gate (1.3e5 m^3/s, Table 1) during the March 2016 measurement campaign. Another way to view this is to recognize that the volume of water delivered by watershed runoff is small compared to the tidal prism for the bay.

Observed suspended-sediment flux at the estuary-ocean boundary of San Francisco Bay following the 2017 peak in wet season freshwater flow from the watershed was larger in magnitude across the range of observed water flux than that following the 2016 watershed flow peak (Fig. 18). In the scatter plot of water flux (Q) and suspended-sediment flux (Qs, Fig. 18), a similar relationship is observed for the March 2016, June 2016, and Teeter et al. (1996) datasets. For the March 2016 and June 2016 field campaigns, the range of observed water flux was similar, and, for a given water flux, similar suspended-sediment flux was observed. In contrast, the water flux vs sediment flux relationship for the February 2017 dataset is more similar to that

for the Erikson et al. (2013) dataset; the slope of the relationship is steeper on flood and ebb tides, meaning that for a given water flux magnitude, the suspended-sediment flux magnitude was greater during the February 2017 and Erikson et al. (2013) field campaigns than the March 2016, June 2016, and Teeter et al. (1996) field campaigns (Fig. 18). Interestingly, Erikson et al. (2013) observations were made during a weaker watershed outflow event (peak Delta outflow was 1450 m^3/s during January 2008, compared to 4100 and 10,700 m^3/s during March 2016 and February 2017, respectively) and also a drier year (daily Delta outflow during 2008 was lower than the long-term mean for the entire year, see Erikson et al., 2013). Higher ambient SSC in Central SFB is one explanation for a steeper slope in the relationship between water flux and suspended-sediment flux, since higher SSC would give rise to higher suspended-sediment flux across all water flux values. This appears to be a likely explanation since mean SSC at Alcatraz (an indicator of SSC in Central SFB) for the 30 days surrounding peak Delta outflow was higher for January 2008 (mean SSC for period 24 Dec 2007 – 23 Jan 2008 = 30.7 mg/L) and February 2017 (mean SSC for period 28 Jan 2017 – 27 Feb 2017 = 46.4 mg/L) than for March 2016 (mean SSC for period 1 Mar 2016 – 31 Mar 2016 = 19.2 mg/L). It is unclear why Central Bay SSC was higher during January 2008 than March 2016 considering the peak Delta outflow was larger for the latter and the Delta outflow peaks were the first of the water year for both years; perhaps the spilling of the Yolo Bypass in 2016 but not in 2008 caused trapping of some the sediment mass from the watershed within the bypass, producing a broader signal with reduced peak SSC flowing into SFB in 2016. Given the similarity in the February 2017 and Erikson et al. (2013) datasets with respect to the Q versus Qs relationship, despite the substantially different Delta outflow conditions, one observation is that peak Delta outflow does not appear to be a particularly good measure of the intensity of a watershed discharge event nor a predictor of sediment outflow at the Golden Gate. Teeter et al. (1996) suggested greater Qs for Q exceeding 50,000 m^3/s, which was not observed in this study nor clearly reflected in the Erikson et al. (2013) dataset.

During the February 2017 field campaign, the longer period of continuous sampling allowed for direct comparison of sediment flux between one ebb and the subsequent flood tide. Interestingly, suspended-sediment flux integrated over each phase of the tide showed 20% less sediment mass leaving SFB on the ebb tide than entering SFB on the subsequent flood tide, despite greater water flux on the ebb tide. This result, indicating more sediment entering SFB than exiting over

one tidal cycle in February 2017, is somewhat surprising given the magnitude of the flows of water and sediment that were entering SFB from the watershed during this period. One explanation for the lower magnitude of ebb-directed sediment flux is the field campaign was conducted after the passing of the peak of the watershed-sourced sediment plume through the estuary and into the Pacific Ocean; if the peak SSC had already passed through the Golden Gate, there would be higher SSC outside the Gate which could cause a landward concentration gradient in suspended sediment. Another explanation for the lower magnitude of ebb-directed sediment flux is decreased SSC in the water column during the ebb tide, caused by vertical stratification at the estuary-ocean boundary which inhibits vertical mixing. This vertical stratification could be a version of strain-induced periodic stratification (or SIPS, Simpson et al., 1990) caused by a near-surface water mass of less-dense watershed outflow underlain by denser ocean water. During the flood tide, stratification is broken down by tidal stirring (Simpson et al., 1990). This result again reveals the challenges of performing field data collection at this site and also the complexity of the interactions between the mean flows and the tidally forced flows, and the difficulties associated with measuring mean quantities within a signal having large deviations from the mean values.

Trapping of watershed sediment pulses in SFB

For both wet season field campaigns (March 2016 and February 2017), we hypothesize that substantial trapping of watershed-sourced pulses of sediment occurred within SFB, specifically San Pablo Bay (Fig. 1), although the time scale of this trapping is unknown. Interestingly, the observed suspended-sediment flux following the 2016 peak in wet season freshwater flow from the watershed closely resembled that during the 2016 dry season in terms of magnitude and relation to water flux (Tables 3-4 and Fig. 18). The observation that the sediment outflow following the March 2016 storm was so similar to June 2016 conditions was initially unexpected considering the magnitude of the March storm—flood water discharge into Yolo Bypass reached a peak not seen since 2011. Monitoring stations in the estuary indicated the movement and apparent trapping of a sediment pulse following the March 2016 storm: elevated SSC was observed to enter SFB at Benicia Bridge with a smaller peak was observed passing San Pablo Bay at Richmond Bridge; but SSC near the estuary-ocean boundary at Alcatraz Island exhibited

very little change (Fig. 5), suggesting limited watershed sediment outflow at the Golden Gate following the March 2016 storm.

Despite the high freshwater flows and flooding of the Yolo Bypass in March 2016, peak observed transect-average SSC at the Golden Gate during March 2016 sampling was not greater than that during June 2016; in fact the peak transect-average SSC during March was 20% lower than that during June (Table 1). This observation of relatively low SSC during the March 2016 campaign could be explained by too much lag between the Delta outflow peak and the campaign (thus missing the peak SSC of the freshwater plume); however inspection of the Alcatraz tidally filtered SSC (Fig. 5C) (and assuming that conditions at Alcatraz are a reasonable surrogate for conditions at the Golden Gate) shows that although the tidally filtered SSC peak (34 mg/L on 8 Mar 2016) occurred earlier than the field campaign (21 mg/L on 21 Mar 2016), tidally filtered peak values during June 2016 were only slightly lower (29 mg/L on 5 Jun 2016). These results suggest that there was not a large amount of sediment export during the 2016 storms. In contrast, the peak observed transect-average SSC at the Golden Gate during February 2017 sampling was nearly double that observed in the previous two field trips (Table 1). Comparing transect data to Alcatraz shows again that the tidally filtered SSC peak (86 mg/L on 21 Feb 2017) occurred earlier than the field campaign (43 mg/L on 27 Feb 2017); however tidally filtered SSC decreased to a summer baseline similar to 2016 (31 mg/L on 26 May 2017).

During 2017, tidally filtered SSC at Benicia Bridge, an indicator of watershed sediment discharge, had a peak value that was nearly equal to that observed in 2016 (~200 mg/L, Figs. 5C & 6C). There were two major peaks in tidally filtered SSC at Benicia Bridge in 2017, whereas during 2016 there was only one (Figs. 5C & 6C), which indicates greater sediment discharge into SFB in 2017 and likely explains the greater tidally filtered SSC observed at Alcatraz and greater transect-average SSC observed at the Golden Gate transect during February 2017 (range of transect-average SSC: 38 – 64 mg/L, Table 1) compared to March 2016 (range of transect-average SSC: 17 – 27 mg/L, Table 1). A striking difference between 2016 and 2017 is seen in tidally filtered SSC at Richmond Bridge. During 2016, tidally filtered SSC at the Richmond Bridge near-bed sensor was at an intermediate value between Benicia Bridge upstream and Alcatraz Island downstream (Fig. 5C). However during 2017, tidally filtered SSC at the near-bed sensor reached peak values of 600 mg/L, three times greater than that observed at Benicia Bridge

during 2017 (Fig. 6C) and about six times greater than that observed at Richmond Bridge during 2016 (Fig. 5C). Comparison of tidally filtered salinity at SFB stations between 2016 and 2017 shows the presence of stratified conditions at Richmond Bridge during February 2017—during 2016 tidally filtered salinity at Richmond Bridge near-bed sensor was similar to that at Alcatraz Island mid-depth sensor with minimum values of about 20 (Fig. 5B), while during 2017 salinity at Richmond deviated from Alcatraz by increasing from 15 to 25 in early February after a large freshwater pulse entered San Pablo Bay (indicated by Carquinez Bridge near-bed sensor salinity reaching 0, Fig. 6B).

The increase in salinity at Richmond Bridge near the bed relative to Alcatraz at mid depth is indicative of vertical density stratification causing near-surface seaward flow and near-bed landward flow. Comparison of tidally filtered SSC to tidally filtered salinity at Richmond Bridge during Jan – Mar 2017 shows peaks in SSC are concurrent with negative peaks in salinity (Fig. 6B), events that occur during spring tides. During spring tides, tidal excursion is higher and tidal mixing is greater, so this observation can be explained by either 1) the seaward movement of an estuarine turbidity maximum (ETM) located north of Richmond Bridge in San Pablo Bay; or 2) the breakdown of SIPS that set up during the previous neap tides. An ETM is a longitudinal maximum of SSC, and can form by several mechanisms including gravitational circulation or tidal asymmetry of velocity and SSC; ETMs require a varying salinity field but are not associated with one particular salinity (Jay and Musiak, 1994; Schoellhamer, 2001). In SFB, an ETM is present and usually located in Suisun Bay (Schoellhamer, 2001). The extreme freshwater discharge from the Central Valley in February 2017 likely forced the ETM downstream into San Pablo Bay (Figs. 6A-B), which would cause trapping of sediment (Jay and Musiak, 1994) in San Pablo Bay. For 2) above, the breakdown of vertical stratification formed during neap tides would enhance both vertical mixing and resuspension from the bed; greater vertical mixing causes fresher near-surface waters to mix with saltier near-bed waters, producing lower values of salinity compared to neap tide. The breakdown of vertical stratification also increases turbulence which causes increased resuspension of sediment from the bed, increasing SSC compared to neap tide. Because the subtidal or residual velocity is landward near the bed in an estuary (Geyer and MacCready, 2014) and SSC was high near the bed during spring tides in San Pablo Bay (Fig. 6C), net landward transport of sediment likely occurred. Taken in context with the relatively weak watershed discharge event of March 2016, both of these explanations add to the hypothesis

that watershed sediment discharge is trapped within San Pablo Bay following freshwater runoff. Additional analysis is needed to investigate this further. Another unknown is the time scale of the trapping. Given the challenges and expense of field data collection, and the potentially long time scale of trapping of sediment within SFB, development of a surrogate for sediment flux at the Golden Gate is essential to understanding sediment flux at the ocean boundary of SFB.

Suitability of Alcatraz Island SSC as a surrogate for SSC at the Golden Gate

Comparison of instantaneous SSC from Alcatraz with transect-average SSC from ADCP transects at the Golden Gate shows that, for the tidal time scale, there may be only certain conditions for which Alcatraz may be a good surrogate. There is reasonable agreement between Alcatraz SSC and transect-average SSC during the field campaigns in March 2016, June 2016, and most of February 2017 (Fig. 19). However, near the end of ebb during the February 2017 field campaign, elevated SSC at Alcatraz (maximum value ~100 mg/L) is not reflected in the transect-average SSC (concurrent value ~50 mg/L). This difference might indicate that SSC passing Alcatraz was confined to flow in the near-surface region during a period of vertical stratification at the Golden Gate transect; if SIPS was present, it would be most pronounced at the end of ebb tide (Simpson et al., 1990). During large watershed outflow, stratification can develop which cannot be characterized with a single sensor at one depth. This difference may also indicate an insensitivity of the ADCP used to estimate SSC given the high percentage of fine-grained particles; the 600-kHz frequency ADCP used in this study has greater signal attenuation for fine-grained particles (Wall et al., 2006). If the latter is true, then Alcatraz is likely a reasonable surrogate for conditions at the Golden Gate for most or all conditions, and the ADCP-estimated SSC data presented here are biased low. However, if substantial vertical stratification develops at the estuary-ocean boundary, or conditions are otherwise not well mixed, Alcatraz would not be the best choice of surrogate since it only provides data from one depth. Even in this case, data from Alcatraz would still play a valuable role in future model calibration and validation (see *Future Work*). Further analysis of conditions at Alcatraz and the estuary-ocean boundary during 2017 is needed to determine the presence and magnitude of vertical stratification. Note that the present location of the Alcatraz Island station has a total depth of only 5 m relative to mean lower low water (Buchanan and Morgan, 2014) whereas the total depth of the region of SFB between Alcatraz and the landward edge of the Golden Gate inlet

ranges from 30 to 40 m (Dartnell, 2015). Thus the present location of Alcatraz would not allow for placement of an additional sensor at a great enough depth to observe near-bed conditions in Central Bay. Further investigation of a suitable location for a deeper site is needed.

Application of Erikson et al. (2013) surrogate relation for sediment flux

Erikson et al. (2013) compared numerical model estimates of tidally-averaged sediment flux at the Golden Gate to measured SSC and predicted (modeled) tidal currents at Alcatraz Island from January-April 2008 to develop an equation for tidally-averaged Golden Gate sediment flux (F_{GG}):

$$F_{GG}=1.21\times10^{5}[SSC][U]+40.3 \qquad \textit{(Eq. 4)}$$

where [SSC] = measured tidally averaged suspended-sediment concentration at Alcatraz in kg/m^3, [U] is tidally-averaged velocity (ebb positive) computed from tidal constituents by program T-TIDE (Pawlowicz et al., 2002) in m/s. A low pass numerical filter with a 1/25 hour^{-1} cutoff frequency (25-hour tidal averaging) was used to calculate tidally-averaged values. The maximum freshwater inflow during the period in 2008 was 1,450 m^3/s.

The same methodology was applied to the Alcatraz SSC data collected through WY2016 which revealed a methodological problem. Two of the six tidal constituents used have periods slightly greater than 25 hours (Table 5 in Erikson et al., 2013), so they are not removed by the filter. Thus, [U] contains a tidal signal and F_{GG} is not tidally-averaged. U is calculated with T-TIDE and is the sum of tidal constituents so in theory [U]=0. This was confirmed by applying a 30-hour tidal filter to the velocity data and the resulting time series was nearly zero as expected.

Thus, the only driver of F_{GG} during high flow is the tidal asymmetry of SSC because freshwater discharge Q is not considered in the equation. For seaward-directed F_{GG}, the asymmetry required is that SSC is greater on ebb tide than flood tide. This works well for low discharge, presumably less than 1450 m^3/s, for which discharge apparently has only a minor effect on sediment flux. F_{GG} likely underestimates sediment flux during periods of discharge greater than 1450 m^3/s. Unfortunately, the Sacramento River delivers most of its sediment during greater flow (*e.g.*, 82% of the sediment delivered in 31% of the time, Wright and Schoellhamer, 2005). A result is that the interannual variability of calculated sediment flux was small, ranging from 1.1-1.3 Mt/yr with a mean value of 1.2 Mt/yr for WY2004-2010.

In summary, the surrogate sediment flux equation presented in Erikson et al. (2013) is not applicable to flows greater than 1450 m^3/s or possibly less and contains some methodological problems. For the 2016 field campaigns, observed [SSC] at Alcatraz were nearly equivalent (21.5 mg/L in March and 21.8 mg/L in June, Fig. 5C), and the observed suspended-sediment flux at the Golden Gate was similar in both magnitude (Tables 3-4) and relation to water flux (Fig. 18). These observations suggest that the use of Alcatraz SSC as a surrogate for sediment flux at the Golden Gate is a reasonable approach, but further work is required to establish a better reference velocity.

Limitations of the study

One limitation of this study is the frequency of the ADCP—a higher frequency instrument is better suited to observe SSC for the fine-grained sediments typically found in SFB (Wall et al., 2006). However, a lower frequency instrument was required to measure water velocity over the deepest region of the transect. The lower frequency means lower sensitivity to the sediment in the water column, which introduces more uncertainty into the computed sediment fluxes. There is not a simple way around this problem, though, because even using two different instruments – one for water and one for sediment – would leave one with a dataset that does not span the full water column. Despite this limitation, the combination of an acoustic Doppler profiler with *in situ* sampling for suspended-sediment concentrations is an effective way to obtain data for quantification of sediment and water fluxes. The method provides unprecedented spatial resolution compared to techniques available in the past. It is also rapid enough to yield nearly synoptic results for a cross-section on the order of one kilometer in width.

Another limitation is the temporal scope of the dataset. The results provide good vertical resolution through portions of the tidal cycle, but computation of net fluxes requires measurements over longer periods of time. Presently, there is no technique available that can observe velocities and suspended sediments throughout a deep channel cross-section without being physically on-site. The acoustic approach employed here provides very high resolution and relatively rapid measurement capability. But operators have to be on site and in a boat for the duration of the measurement campaign.

Future work

The measurements presented in this report and preferably additional measurements can be used with a numerical model of sediment transport to develop time series of suspended-sediment flux over many years. This would provide estimates of the tidally averaged flux, seasonal fluxes, and annual fluxes, to help "close the loop" on sediment budget calculations in the Bay. The high flow data from 2017 enable development of a more robust time series than that of Erikson et al. (2013). Such an approach would provide suspended-sediment flux time series while not requiring deployment of moored instruments in the Golden Gate cross section, which poses many challenges, including: representing a large and complex cross section with point measurements; likely need for multiple deployments in the cross section to capture spatial variability; physical difficulties including large tidal currents, large swell, high winds, and shipping traffic; and cost. The steps to accomplish this are:

1) Run a well-calibrated numerical suspended-sediment model to estimate SSF at the Golden Gate at the time of the measurements.

2) Compare numerically modeled and measured fluxes. They will not agree probably due to inaccuracy of the model and model inputs, more than the measurements. Determine a regression model to best calculate measured flux from the numerically modeled flux (Fig. 20).

3) Compare the difference between measured and modeled suspended-sediment flux (commonly called residuals) with possible causes of the scatter in Figure 20 to identify sources of error and possibly correct them to make better numerical and regression models. For example, if the numerical model over predicts wind-wave resuspension and resulting export, the model suspended-sediment flux would increase above measured suspended-sediment flux as wind speed increases.

4) Use the best regression to correct the numerical model suspended-sediment flux to develop estimated time series of suspended-sediment flux for the duration of the model run. As the numerical model improves and more data are available, the regression and the suspended-sediment flux time series can evolve and improve.

5) Use the corrected model suspended-sediment flux from 4) to develop a relation between suspended-sediment flux and relevant parameters that are readily available such as SSC at Alcatraz and freshwater flow, similar to the approach of Erikson et al. (2013). This would allow

estimation of suspended-sediment flux at times other than the duration of the model runs. For example, measurement of SSC at Alcatraz started in 2003, so it may be possible to develop suspended-sediment flux time series from 2003 to present.

6) Model results can be used to identify conditions that create large suspended-sediment flux and thus under what conditions additional measurements should be collected.

In conjunction with this modeling effort, additional field measurements during large watershed outflow events are recommended, but with multiple days of measurements for a single storm. In terms of the watershed outflow hydrograph (*e.g.*, Figs. 5A & 6A), conducting several field campaigns over the duration of the hydrograph (*e.g.*, the rising limb, peak, and falling limb) would provide additional data to understand the nature of sediment transport through San Francisco Bay from the watershed to the ocean.

References

Buchanan, P.A., Downing-Kunz, M.A., Schoellhamer, D.H., Shellenbarger, G.G., and Weidich, K.W., 2014. Continuous Water-Quality and Suspended-Sediment Transport Monitoring in the San Francisco Bay, California, Water Years 2011–13, U.S. Geological Survey Fact Sheet 2014-3090. Accessible online at http://dx.doi.org/10.3133/fs20143090.

Buchanan, P.A. and Morgan, T.L., 2014. Summary of suspended-sediment concentration data, San Francisco Bay, California, water year 2010: U.S. Geological Survey Data Series 808, 30 p., http://dx.doi.org/10.3133/ds808.

CDWR (California Department of Water Resources), 1986. DAYFLOW computer program documentation and data summary user's guide. Sacramento, California: California Department of Water Resources, http://www.water.ca.gov/dayflow/documentation.

Chen, C., 1991. Unified Theory on Power Laws for Flow Resistance. *Journal of Hydraulic Engineering* 117: 371-389.

Dartnell, P., 2015. Data integration and visualization, Offshore of San Francisco map area, California, *sheet 4 in* Cochrane, G.R., Johnson, S.Y., Dartnell, P., Greene, H.G., Erdey, M.D., Golden, N.E., Hartwell, S.R., Endris, C.A., Manson, M.W., Sliter, R.W., Kvitek, R.G., Watt, J.T., Ross, S.L., and Bruns, T.R. (G.R. Cochrane and S.A. Cochran, eds.), California State Waters Map Series—Offshore of San Francisco, California: U.S. Geological Survey Open-File Report 2015–1068, pamphlet 39 p., 10 sheets, scale 1:24,000, accessible online at http://dx.doi.org/10.3133/ofr20151068.

Downing-Kunz, M.A., and D.H. Schoellhamer., 2013. Seasonal variations in suspended-sediment dynamics in the tidal reach of an estuarine tributary. *Marine Geology* 435: 314–326.

Edwards, T.K., and Glysson, G.D., 1999. Field methods for measurement of fluvial sediment, in: U.S Geological Survey Techniques of Water-Resource Investigations, book 3, Applications of Hydraulics, chap. C2 (rev.), 89 pp. Available at http://pubs.usgs.gov/twri/twri3-c2/.

Erikson, L.H., Wright, S.A., Elias, E., Hanes, D.M., Schoellhamer, D.H., and Largier, J., 2013. The use of modeling and suspended-sediment concentration measurements for quantifying net

suspended-sediment transport through a large tidally dominated inlet. *Marine Geology* 345: 96-112.

Federal Interagency Sedimentation Project, 2001. The US D-96: An isokinetic suspended-sediment/water-quality collapsible-bag sampler, Interagency Report PP: Vicksburg, MS, Waterways Experiment Station, 37 p.

Gartner, J.W., 2004. Estimating suspended solids concentrations from backscatter intensity measured by acoustic Doppler current profiler in San Francisco Bay, California. *Marine Geology* 211: 169–187.

Ganju, N.K., Schoellhamer, D.H., 2006. Annual sediment flux estimates in a tidal strait using surrogate measurements. *Estuarine, Coastal and Shelf Science* 69: 165–178.

Geyer, W.R. and MacCready, P., 2014. The Estuarine Circulation. *Annual Review of Fluid Mechanics* 46: 175-197.

Jay, D. A., and Musiak, J. D., 1994. Particle trapping in estuarine tidal flows. *Journal of Geophysical Research* 99(C10), 20445-20461.

Landers, M.N., Straub, T.D., Wood, M.S., and Domanski, M.M., 2016. Sediment acoustic index method for computing continuous suspended-sediment concentrations: U.S. Geological Survey Techniques and Methods, book 3, chap. C5, 63 p., http://dx.doi.org/10.3133/tm3C5.

McKee, L.J., Ganju, N.K., Schoellhamer, D.H., 2006. Estimates of suspended sediment entering San Francisco Bay from the Sacramento and San Joaquin Delta, San Francisco Bay, California. *Journal of Hydrology* 323: 335–352.

Pawlowicz R., Beardsley B., Lentz S., 2002. Classical tidal harmonic analysis including error estimates in MATLAB using T_TIDE. *Computers and Geosciences* 28:929−937

Rasmussen, P.P., Gray, J.R., Glysson, G.D., and Ziegler, A.C., 2009. Guidelines and procedures for computing time-series suspended-sediment concentrations and loads from in-stream turbidity-sensor and streamflow data: United States Geological Survey Techniques and Methods, book 3, chap. C4, 52 p.

Ruhl, C.A., Schoellhamer, D.H., Stumpf, R.P., and Lindsay, C.L., 2001. Combined use of remote sensing and continuous monitoring to analyze the variability of suspended-sediment concentrations in San Francisco Bay, California. *Estuarine, Coastal and Shelf Science* 53, p. 801-812.

Schoellhamer, D.H., 2001. Influence of salinity, bottom topography, and tides on locations of

estuarine turbidity maxima in northern San Francisco Bay, in McAnally, W.H. and Mehta, A.J., ed., Coastal and Estuarine Fine Sediment Transport Processes: Elsevier Science B.V., p. 343-357.

Schoellhamer, D.H., 2002. Variability of suspended-sediment concentration at tidal to annual time scales in San Francisco Bay, USA. *Continental Shelf Research* 22: 1857–1866.

Schoellhamer, D.H., Lionberger, M.A., Jaffe, B.E., Ganju, N.K., Wright, S.A., and Shellenbarger, G.G., 2005. Bay Sediment Budgets: Sediment Accounting 101: The Pulse of the Estuary: Monitoring and Managing Water Quality in the San Francisco Estuary, San Francisco Estuary Institute, Oakland, California, p. 58-63.

Simpson, J.H., Brown, J., Matthews, J., and Allen, G., 1990. Tidal Straining, Density Currents, and Stirring in the Control of Estuarine Stratification. *Estuaries* 13: 125-132.

Simpson, M.R. and Oltmann, R.N., 1990. An Acoustic Doppler Discharge Measurement System: Proceedings of the 1990 National Conference on Hydraulic Engineering, Vol. 2, p. 903-908.

Teeter, A.M., Letter, J.V., Pratt, T.C., Callegan, C.J., Boyt, W.L., 1996. San Francisco Bay long-term management strategy (LTMS) for dredging and disposal. Report 2. Baywide suspended sediment transport modeling. Technical Report #A383413. Army Engineer Waterways Experiment Station, Hydraulics Lab, Vicksburg, MS.

Teledyne RD Instruments, 2016. WinRiver II Software User's Guide. P/N 957-6231-00. 298 p.

Wall, G.R., Nystrom, E.A., and Litten, S., 2006. Use of an ADCP to compute suspended-sediment discharge in the tidal Hudson River, New York: U.S. Geological Survey Scientific Investigations Report 2006-5055, 16 p.

Wright, S.A., and D.S. Schoellhamer., 2005. Estimating sediment budgets at the interface between rivers and estuaries with application to the Sacramento-San Joaquin River Delta. *Water Resources Research* 41, W09428.

Tables

Table 1. Summary of field campaign dates, conditions, range of observed transect-average suspended-sediment concentration (SSC), and peak freshwater inflow preceding sampling.

Sampling date	Conditions	Range of observed transect-average SSC at Golden Gate (mg/L)	Peak of daily Delta ouflow prior to sampling (value in m^3/s, date)
21-22 March 2016	High inflow	16.7 - 27.0	4100, 3/16/16
23 June 2016	Summer; low flow	18.9 - 34.8	200, 6/20/16
27 Feb 2017	High inflow	37.6 - 63.9	10700[1], 2/12/17

[1]Preliminary data from CDWR via California Data Exchange Center station DTO, subject to revision (cdec.water.ca.gov).

Table 2. Comparison of water sampling methods and calibration curve regression parameters (Eqs. 2 and3) developed for the 2016 and 2017 field campaigns; b_0: y-intercept; b_1: slope; BCF: bias correction factor; R^2: coefficient of determination. See Methods section for description of the sampling methods. The March 2016 regression model was not applied in this study and is shown for comparison purposes only.

Field campaign	Water sampling method	b_0	b_1	BCF	R^2
March 2016	Depth-integrated (D-96)	-2.45	0.044	1.06	0.55
June 2016	Point-integrated (P-61)	-2.68	0.048	1.02	0.91
February 2017	Point-integrated (P-61)	-1.91	0.040	1.03	0.89

Table 3. March 2016 ADCP transects: date (format: month/day/year); start and end times of each transect (time zone: Pacific Standard Time, PST); observed tidal stage (datum: mean sea level, MSL) at San Francisco, CA (station 9414290); computed volumetric water flux; computed suspended-sediment flux; and mean suspended-sediment concentration (SSC) for the transect. Positive flux indicates ebb-tide directed transport; negative flux indicates flood-tide directed transport.

Date	Start Time (PST)	End Time (PST)	Tidal Stage (m MSL)	Water flux (m^3/s)	Sediment flux (kg/s)	Sediment flux (kg/min)	Transect-average SSC (mg/L)
3/21/16	10:22	10:50	0.85	-49800	-720	-43200	19.7
3/21/16	11:33	12:12	0.69	34300	653	39180	18.7
3/21/16	12:37	13:04	0.37	87200	1440	86400	18.4
3/21/16	13:11	13:39	0.15	115900	1200	72000	17.2
3/21/16	13:43	14:13	-0.08	129600	1440	86400	17.6
3/21/16	14:17	14:43	-0.32	125500	1650	99000	25.2
3/21/16	14:50	15:18	-0.49	119500	2110	126600	22.7
3/21/16	15:19	15:45	-0.60	103600	1460	87600	20.5
3/21/16	15:52	16:17	-0.68	89900	1320	79200	16.9
3/21/16	16:18	16:45	-0.70	67200	894	53640	25.0
3/21/16	17:07	17:33	-0.60	31800	495	29700	16.9
3/22/16	07:49	08:36	0.07	-96500	-1940	-116400	25.7
3/22/16	08:46	09:18	0.34	-100900	-2070	-124200	25.0
3/22/16	09:21	09:52	0.52	-100600	-1920	-115200	27.0
3/22/16	09:53	10:18	0.61	-90300	-1380	-82800	22.7
3/22/16	10:21	10:51	0.66	-75700	-1350	-81000	22.2
3/22/16	10:56	11:23	0.69	-46300	-772	-46320	19.7
3/22/16	11:24	11:49	0.66	-26600	-381	-22860	16.7

Table 4. June 2016 ADCP transects: date (format: month/day/year); start and end times of each transect (time zone: Pacific Standard Time, PST); observed tidal stage (datum: mean sea level, MSL) at San Francisco, CA (station 9414290); computed volumetric water flux; computed suspended-sediment flux; and mean suspended-sediment concentration (SSC) for the transect. Positive flux indicates ebb-tide directed transport; negative flux indicates flood-tide directed transport.

Date	Start Time (PST)	End Time (PST)	Tidal Stage (m MSL)	Water flux (m^3/s)	Sediment flux (kg/s)	Sediment flux (kg/min)	Transect-average SSC (mg/L)
6/23/16	06:27	06:47	-0.95	117700	1610	96600	20.6
6/23/16	06:48	07:12	-1.08	107400	1620	97200	20.4
6/23/16	07:13	07:33	-1.09	85800	1310	78600	18.9
6/23/16	07:35	08:01	-1.13	74700	1260	75600	19.1
6/23/16	09:22	09:45	-0.78	-70300	-621	-37200	26.2
6/23/16	10:53	11:24	-0.25	-108600	-2130	-127800	32.7
6/23/16	11:26	11:51	-0.07	-109600	-2130	-127800	29.7
6/23/16	11:52	12:22	0.09	-110100	-1990	-119400	34.8
6/23/16	12:53	13:17	0.33	-110900	-1890	-113400	32.3

Table 5. February 2017 ADCP transects: date (format: month/day/year); start and end times of each transect (time zone: Pacific Standard Time, PST); observed tidal stage (datum: mean sea level, MSL) at San Francisco, CA (station 9414290); computed volumetric water flux; computed suspended-sediment flux; and mean suspended-sediment concentration (SSC) for the transect. Positive flux indicates ebb-tide directed transport; negative flux indicates flood-tide directed transport.

Date	Start Time (PST)	End Time (PST)	Tidal Stage (m MSL)	Water flux (m^3/s)	Sediment flux (kg/s)	Sediment flux (kg/min)	Transect-average SSC (mg/L)
2/27/17	9:53	10:25	0.63	-105300	-3470	-208200	48.1
2/27/17	10:25	10:54	0.76	-98900	-2600	-156000	49.7
2/27/17	11:06	11:33	0.87	-76600	-2560	-153600	43.6
2/27/17	11:35	12:00	0.92	-53900	-1390	-83400	43.3
2/27/17	12:34	12:58	0.85	-100	109	6540	39.1
2/27/17	12:59	13:26	0.79	33600	1190	71400	40.7
2/27/17	13:26	13:49	0.68	59100	1930	115800	40.2
2/27/17	13:51	14:15	0.55	93600	2640	158400	37.8
2/27/17	14:17	14:36	0.34	102200	2530	151800	39.5
2/27/17	14:55	15:27	0.04	121000	3830	229800	40.8
2/27/17	16:03	16:22	-0.45	99400	3040	182400	49.9
2/27/17	16:29	16:54	-0.57	124300	2960	177600	58.7
2/27/17	17:17	17:36	-0.70	102200	2460	147600	45.5
2/27/17	17:37	18:01	-0.74	79300	2140	128400	45.6
2/27/17	18:34	18:53	-0.7	46200	1710	102600	38.3
2/27/17	18:54	19:26	-0.64	16300	525	31500	45.1
2/27/17	19:33	20:00	-0.56	-13200	-973	-58380	47.6
2/27/17	20:02	20:23	-0.44	-41300	-1930	-115800	47.5
2/27/17	20:24	20:47	-0.31	-60200	-2910	-174600	47.4
2/27/17	20:48	21:10	-0.17	-81400	-3740	-224400	52.2
2/27/17	21:11	21:33	-0.05	-93700	-4630	-277800	47.2
2/27/17	21:34	22:01	0.06	-111200	-4230	-253800	54.3
2/27/17	22:03	22:30	0.2	-113600	-5390	-323400	57.7
2/27/17	22:30	22:56	0.35	-114300	-4780	-286800	61.7
2/27/17	22:59	23:27	0.48	-112900	-5830	-349800	63.9
2/27/17	23:28	23:52	0.58	-99300	-3920	-235200	58.5

2/27/17	23:53	0:17	0.67	-84600	-3070	-184200	50.9
2/28/17	0:17	0:40	0.72	-67700	-1850	-111000	46.9
2/28/17	0:41	1:06	0.76	-53200	-1430	-85800	41.9
2/28/17	1:07	1:31	0.76	-19000	-383	-22980	44.7
2/28/17	1:34	2:00	0.70	8400	319	19140	42
2/28/17	2:02	2:30	0.61	43100	1510	90600	37.6

Figures

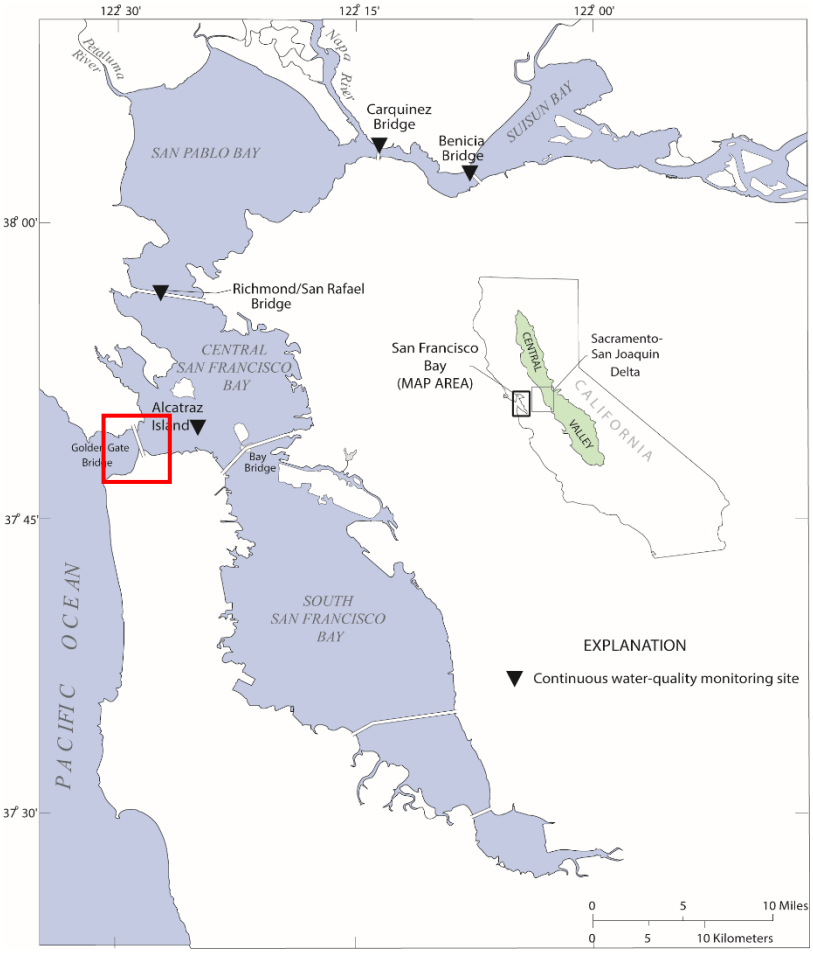

Figure 1. Map of San Francisco Bay, with location of field measurements near Golden Gate inlet (red box) and water-quality monitoring stations used in this study (inverted triangles)—Benicia Bridge (USGS station ID 11455780), Carquinez Bridge (USGS station ID 11455820), Richmond/San Rafael Bridge (USGS station ID 375607122264701), and Alcatraz Island (USGS station ID 374938122251801).

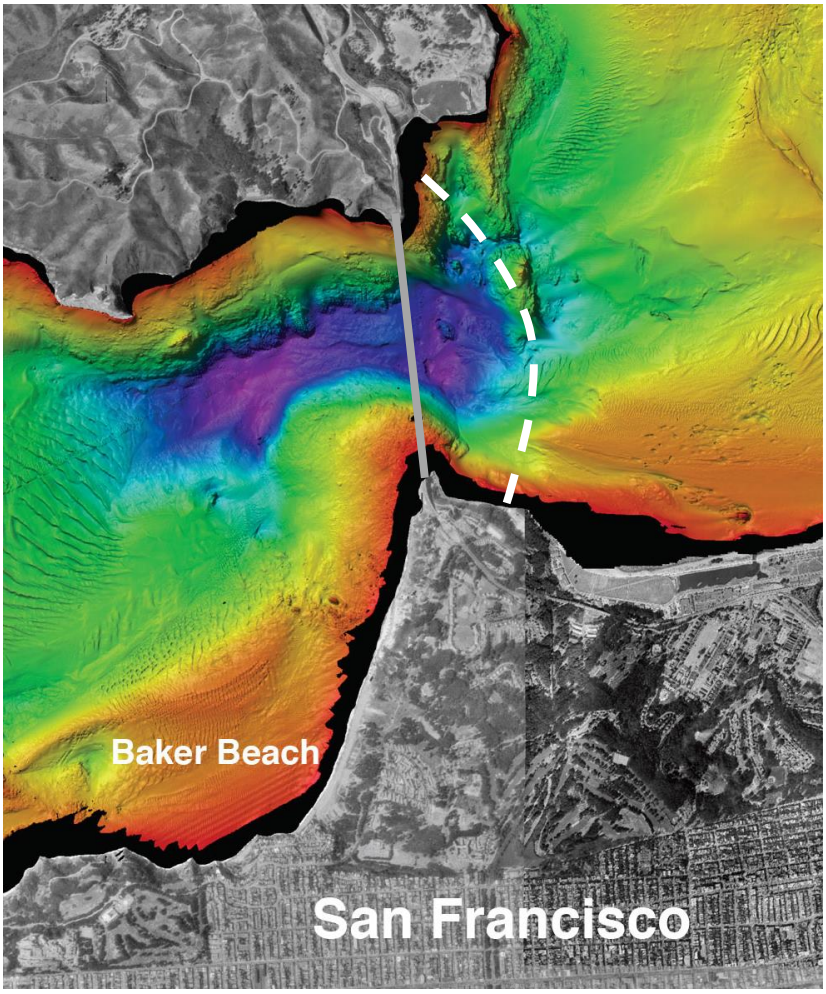

Figure 2. Color shaded-relief bathymetry map of the Golden Gate inlet (red box in Fig. 1), from Dartnell (2015). Colors show depth: reds and oranges indicate shallower areas; purples indicate deeper areas (> 100 m depth). Golden Gate Bridge denoted by thick gray line at narrowest width of inlet. Vessel-based measurements were collected along a defined transect indicated by the white dashed line just east of the bridge.

Figure 3. Down-looking ADCP installed on the R/V Questuary in March 2016. Instrument was lowered below water surface for measurements.

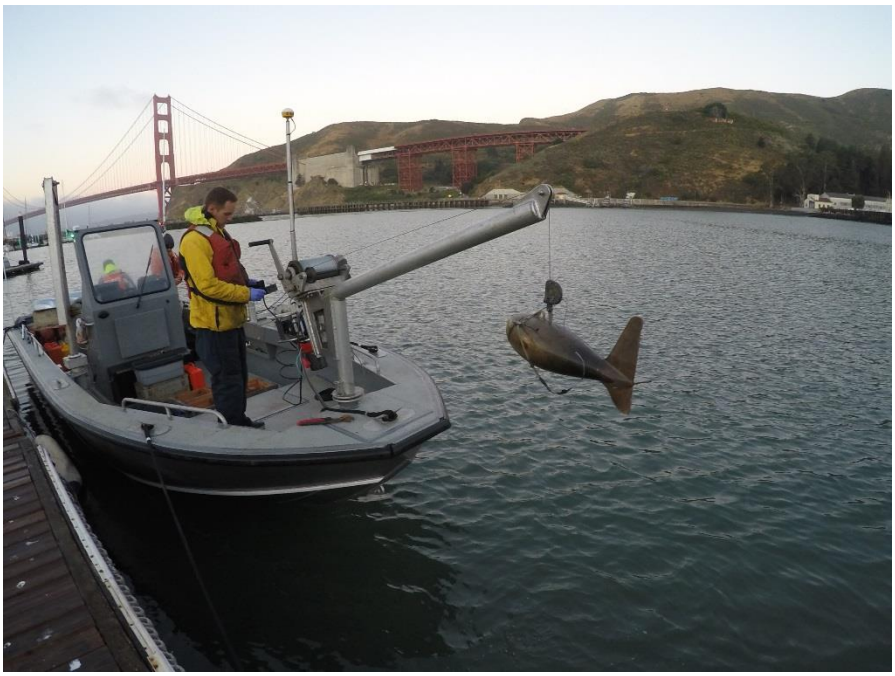

Figure 4. R/V Dinehart and sampling boom equipped with P-61 point-integrating sampler for determining suspended-sediment concentration in June 2016.

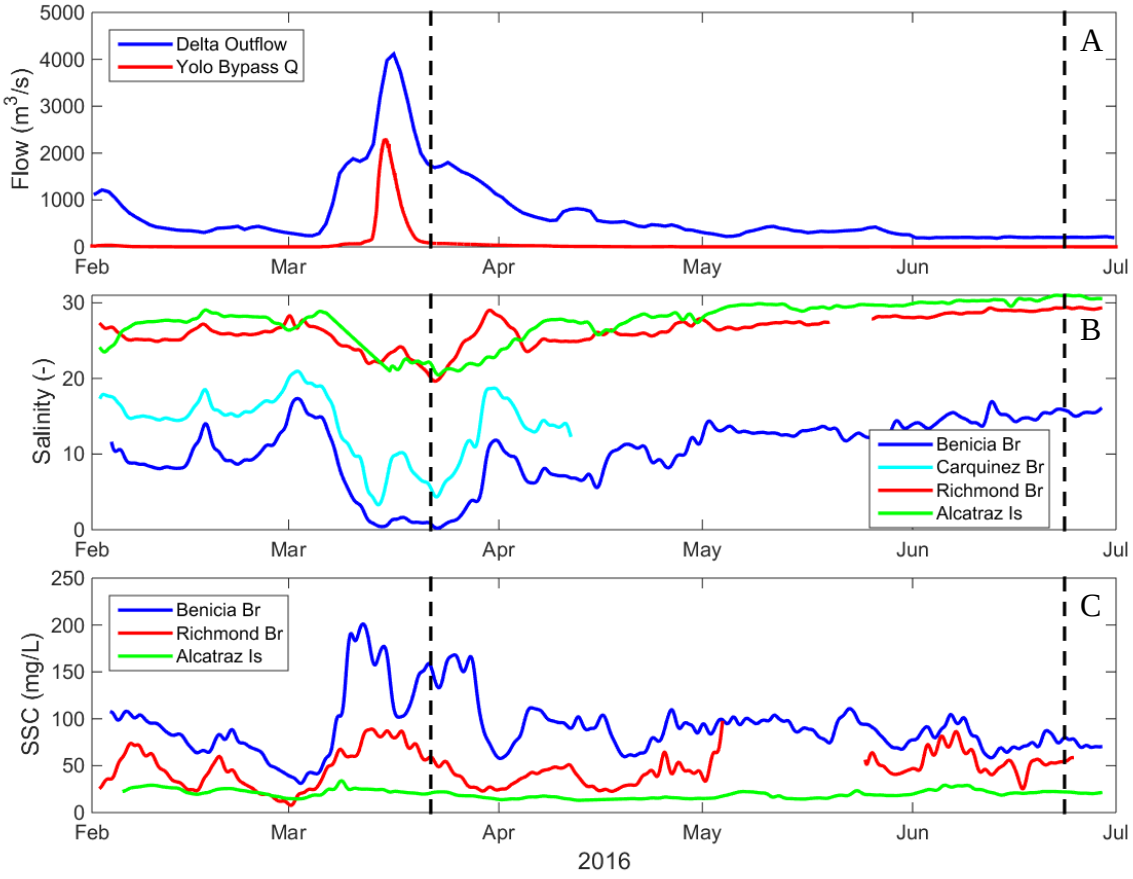

Figure 5. 2016 time series of (A) estimated (DAYFLOW) freshwater flow from Delta to San Francisco Bay ('Delta Outflow') and flow into Yolo Bypass flood control structure and tidally filtered (B) salinity and (C) suspended-sediment concentration (SSC) at four and three San Francisco Bay stations, respectively. Near-bed sensor data shown for Benicia, Carquinez (salinity only), and Richmond stations; mid-depth sensor data shown for Alcatraz. Vertical dashed lines denote midpoint of wet season (21 Mar 2016 23:05:30 PST) and dry season (23 Jun 2016 09:52:00 PST) field campaigns.

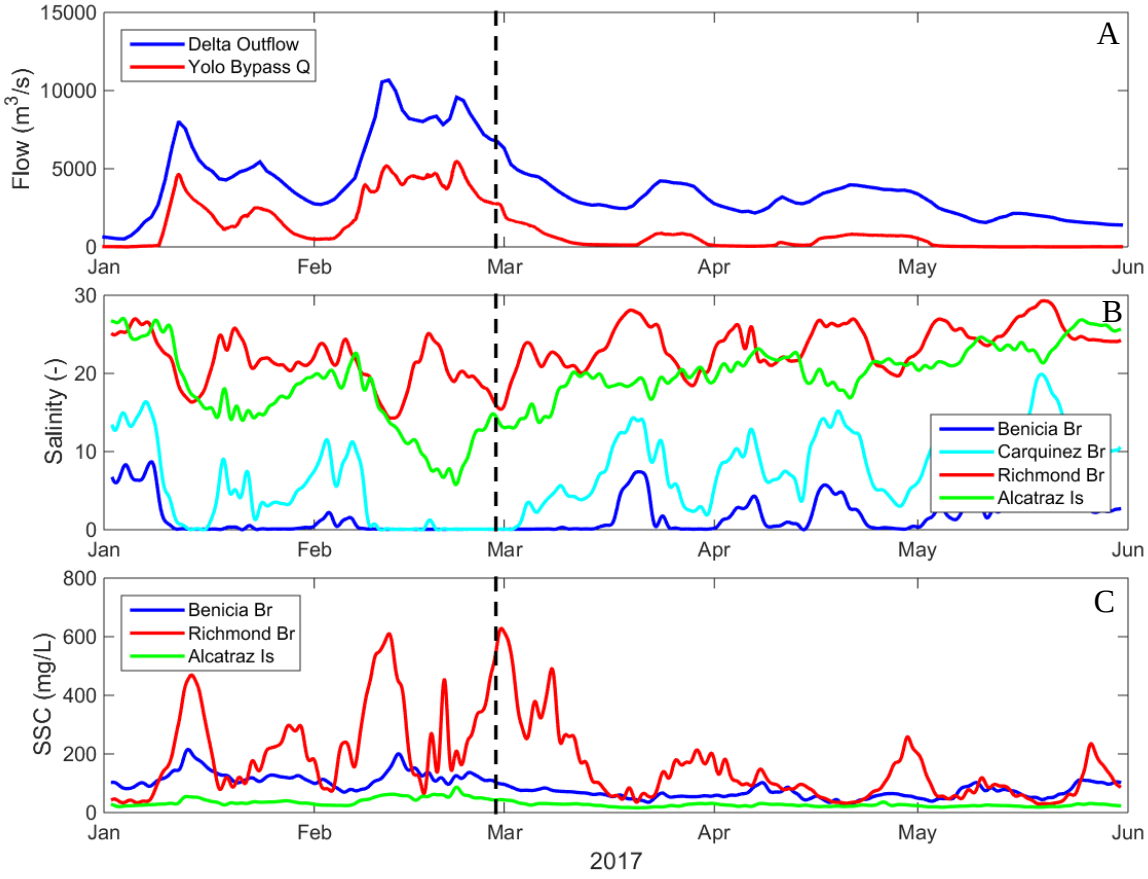

Figure 6. 2017 time series of (A) estimated (DAYFLOW) freshwater flow from Delta to San Francisco Bay ('Delta Outflow') and flow into Yolo Bypass flood control structure and tidally filtered (B) salinity and (C) suspended-sediment concentration (SSC) at four and three San Francisco Bay stations, respectively. Near-bed sensor data shown for Benicia, Carquinez (salinity only), and Richmond stations; mid-depth sensor data shown for Alcatraz. Vertical dashed line denotes midpoint of wet season field campaign (27 Feb 2017 19:00:00 PST).

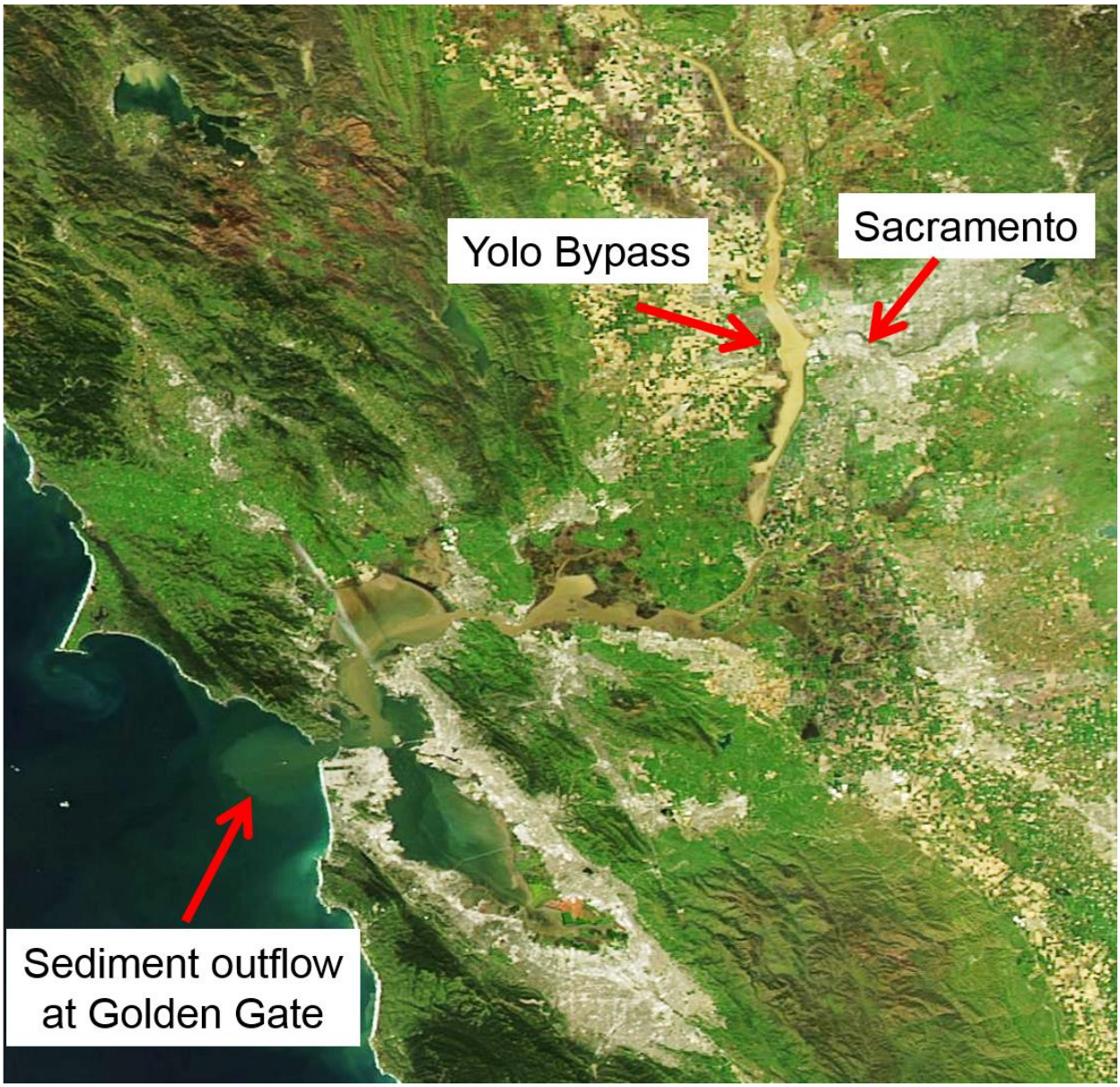

Figure 7. Satellite image from MODIS taken on 16 Mar 2016 at approximately 1222 PST. Low tide at the Golden Gate occurred at 1212 PST (https://tidesandcurrents.noaa.gov/waterlevels.html?id=9414290), essentially the same time as the image. Slack after ebb tide was predicted at 1336 PST, so the tide was still ebbing when this image was taken (https://tidesandcurrents.noaa.gov/noaacurrents/Predictions?id=SFB1202) Visible in this image are sediment-laden water entering San Francisco Bay from the Upper Sacramento River, a flooded Yolo Bypass near Sacramento, CA, and a faint sediment plume at the ocean boundary of San Francisco Bay indicating sediment outflow at the Golden Gate. Source: worldview.earthdata.nasa.gov

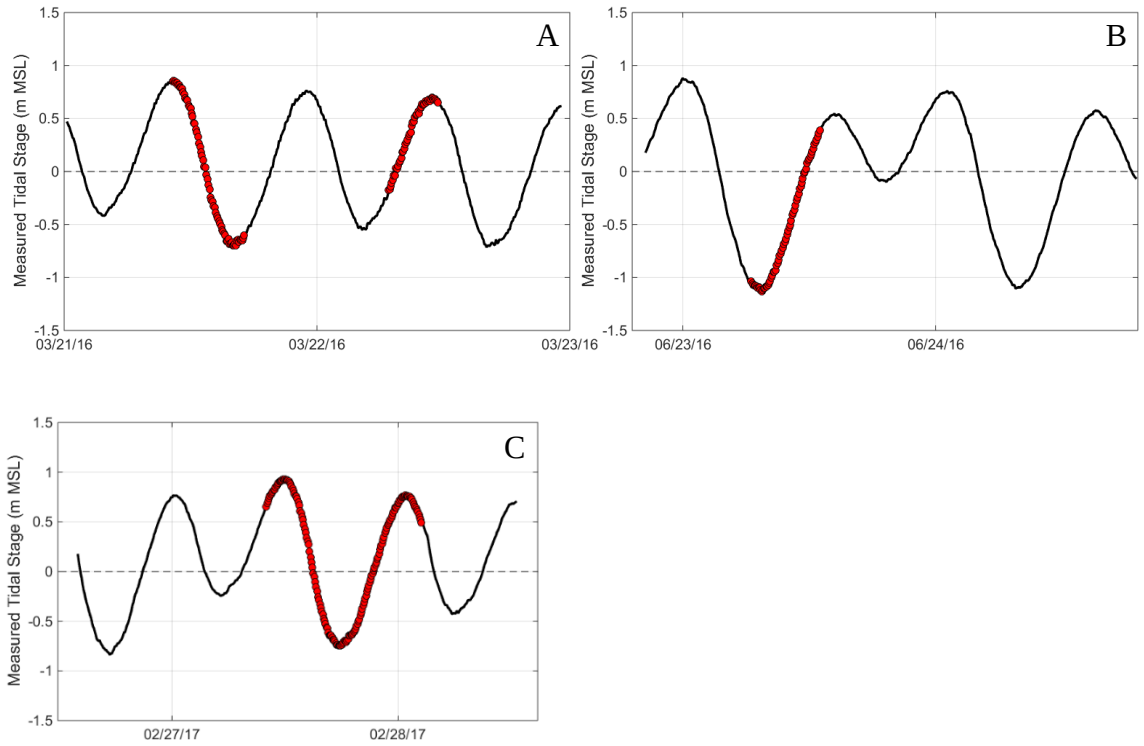

Figure 8. Measured tidal stage (in m relative to mean sea level, MSL) at San Francisco, CA (NOAA station ID 9414290) for field measurements in 2016: 21-22 March (A) and 23 June (B); and in 2017: 27-28 Feb (C). Period of ADCP transecting for discharge and sediment flux calculation indicated by colored circles.

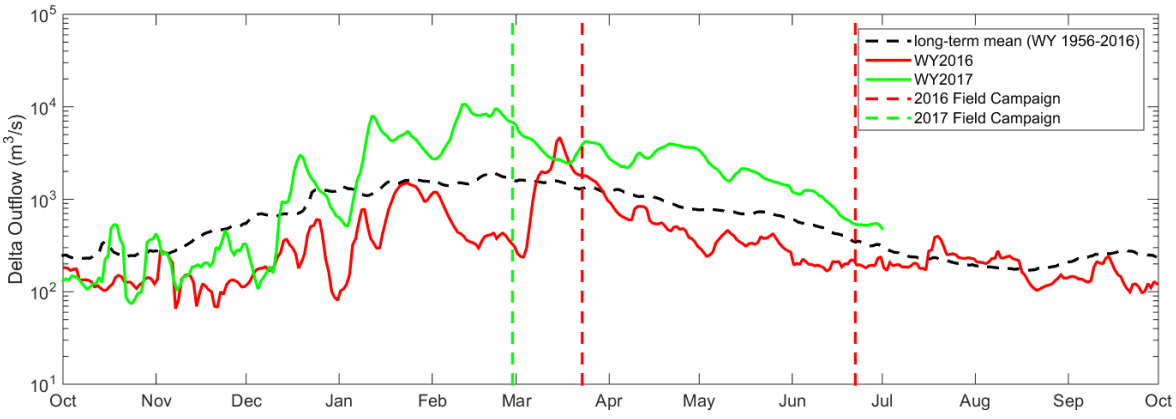

Figure 9. Comparison of water year (WY) 2016 (in red) and 2017 (in green) modeled daily Delta Outflow to long-term mean daily values from WY 1956-2016 (dashed dark line). Vertical dashed lines denote midpoint of 2016 wet season (21 Mar 2016 23:05:30 PST, in red), 2016 dry season (23 Jun 2016 09:52:00 PST, in red), and 2017 wet season (27 Feb 2017 19:00:00 PST, in green) field campaigns.

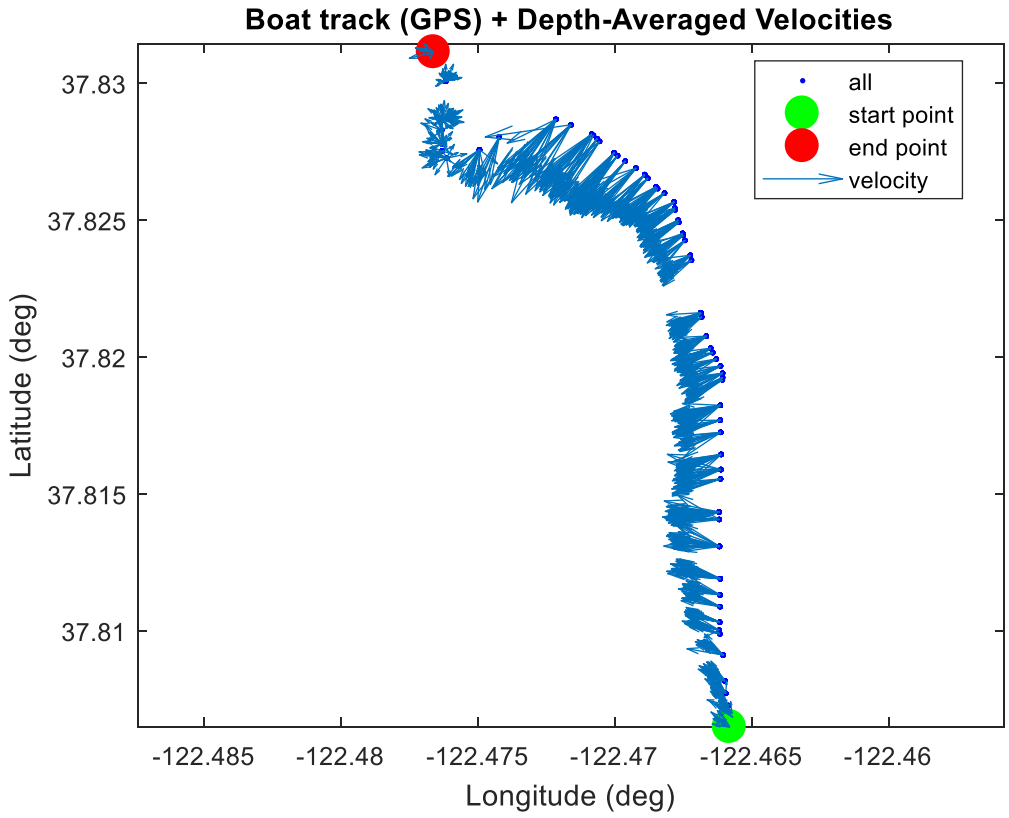

Figure 10. Ship track and velocity vectors along the ADCP transect (Fig. 2) collected on 21 Mar 2016 with start time 13:11 PST. Velocity vectors show magnitude and direction of the depth-averaged currents (ebb-tide directed flow is nominally to the left in the figure), without any interpolation to fill the data gaps that resulted from instrument communication problems.

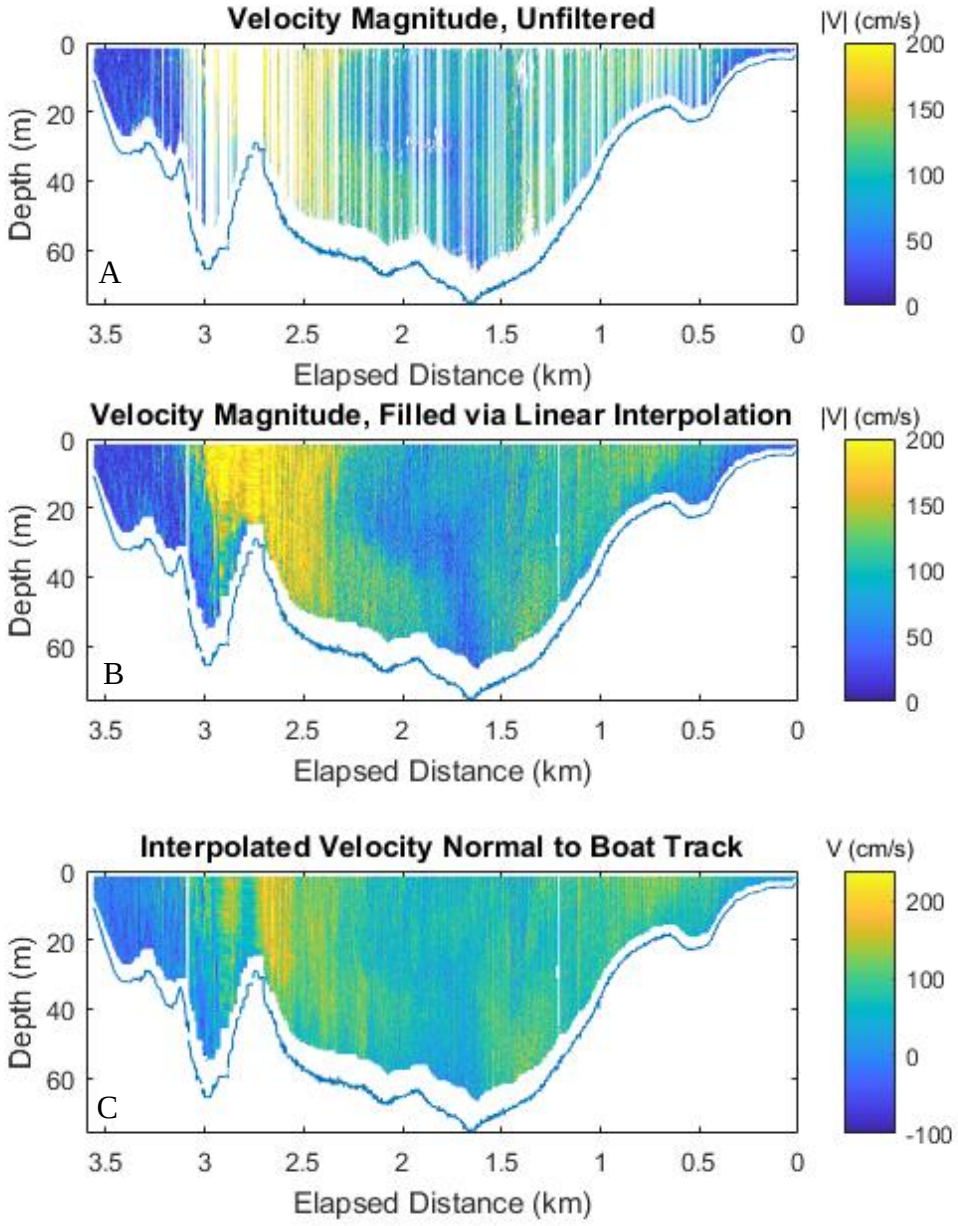

Figure 11. Cross-sectional view of raw (A) and interpolated (B) velocity magnitude, and track-normal velocity component (C), for the transect beginning 13:11 PST on 21 Mar 2016. Velocity is in cm/s; positive values indicate ebb-directed flow. Left edge of plots correspond to north end of transect. Maximum gap of 50 m used for interpolation.

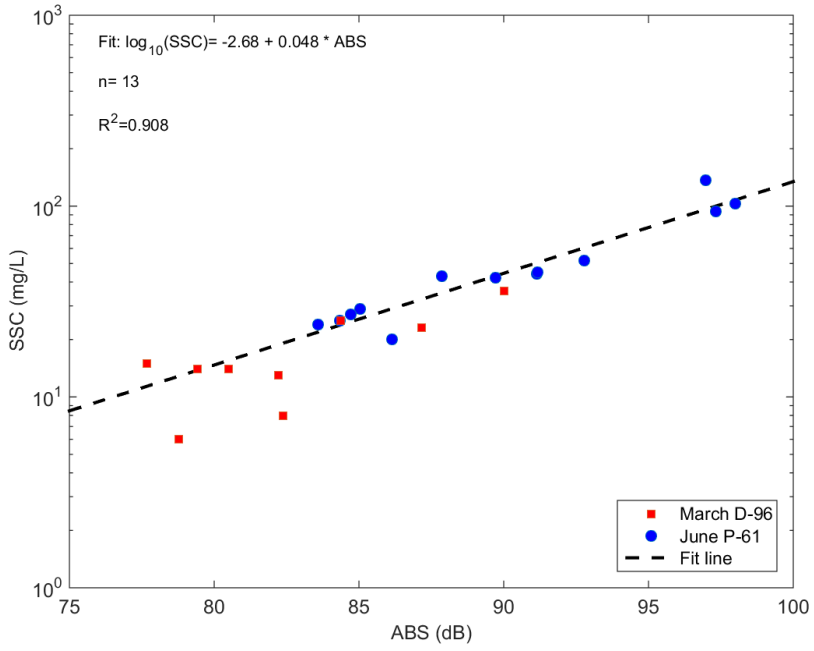

Figure 12. Calibration curve relating sediment-corrected acoustic backscatter (ABS, in decibels) to suspended-sediment concentration (SSC, in milligrams per liter) for 2016 measurements. Water samples from March 2016 (red squares) were collected using a depth-integrated sampler (D-96), while those from June 2016 (blue circles) were collected using a point - integrated sampler (P-61); the same ADCP was used to obtain ABS for both datasets. Fit line shown is the result of ordinary least squares regression analysis of June 2016 samples only; March 2016 samples are shown for comparison between the two datasets.

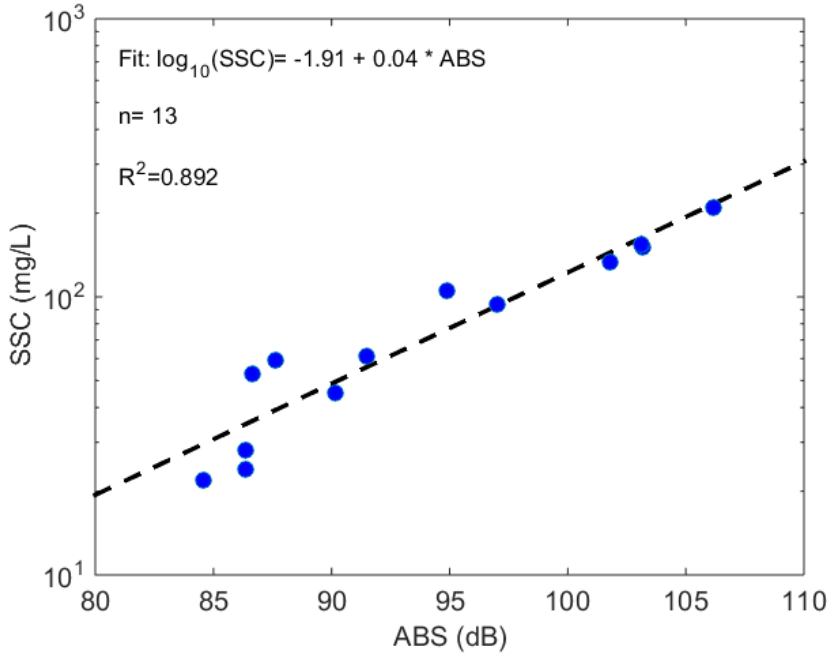

Figure 13. Calibration curve relating sediment-corrected acoustic backscatter (ABS, in decibels) to suspended-sediment concentration (SSC, in milligrams per liter) for 2017 measurements. Water samples from February 2017 (blue circles) were collected using a point-integrated sampler (P-61). Fit line shown is the result of ordinary least squares regression analysis of February 2017 samples only.

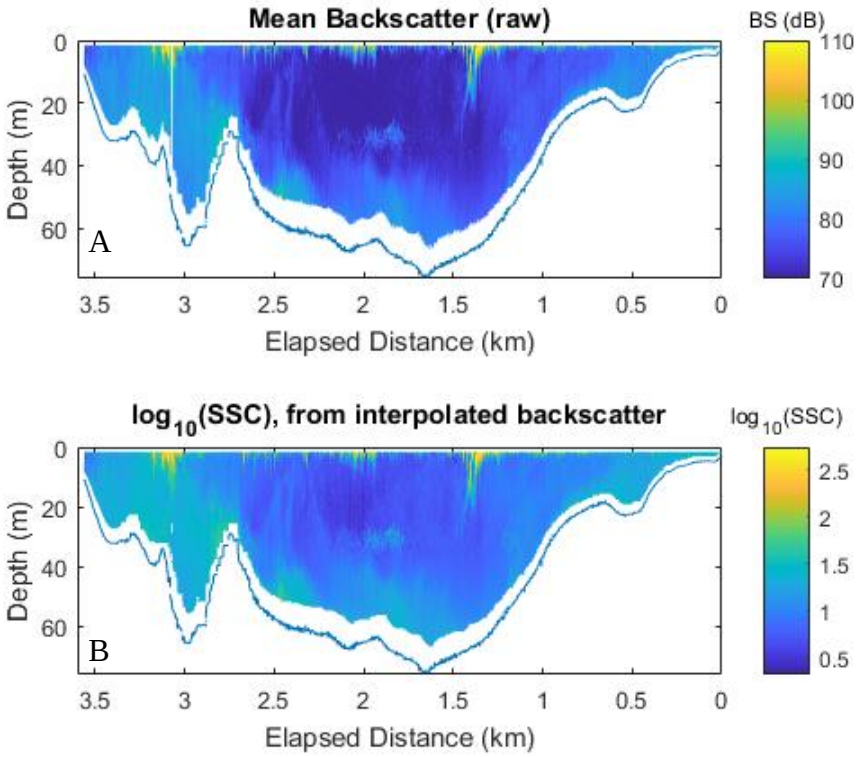

Figure 14. Cross-sectional view of (A) 4-beam average sediment-corrected acoustic backscatter (BS, decibels), and (B) log-transformed suspended-sediment concentration (SSC, mg/L), computed from observed sediment-corrected acoustic backscatter via regression model (Table 2). Data shown are from the transect beginning 13:11 PST on 21 Mar 2016. Left edge of plots correspond to north end of transect.

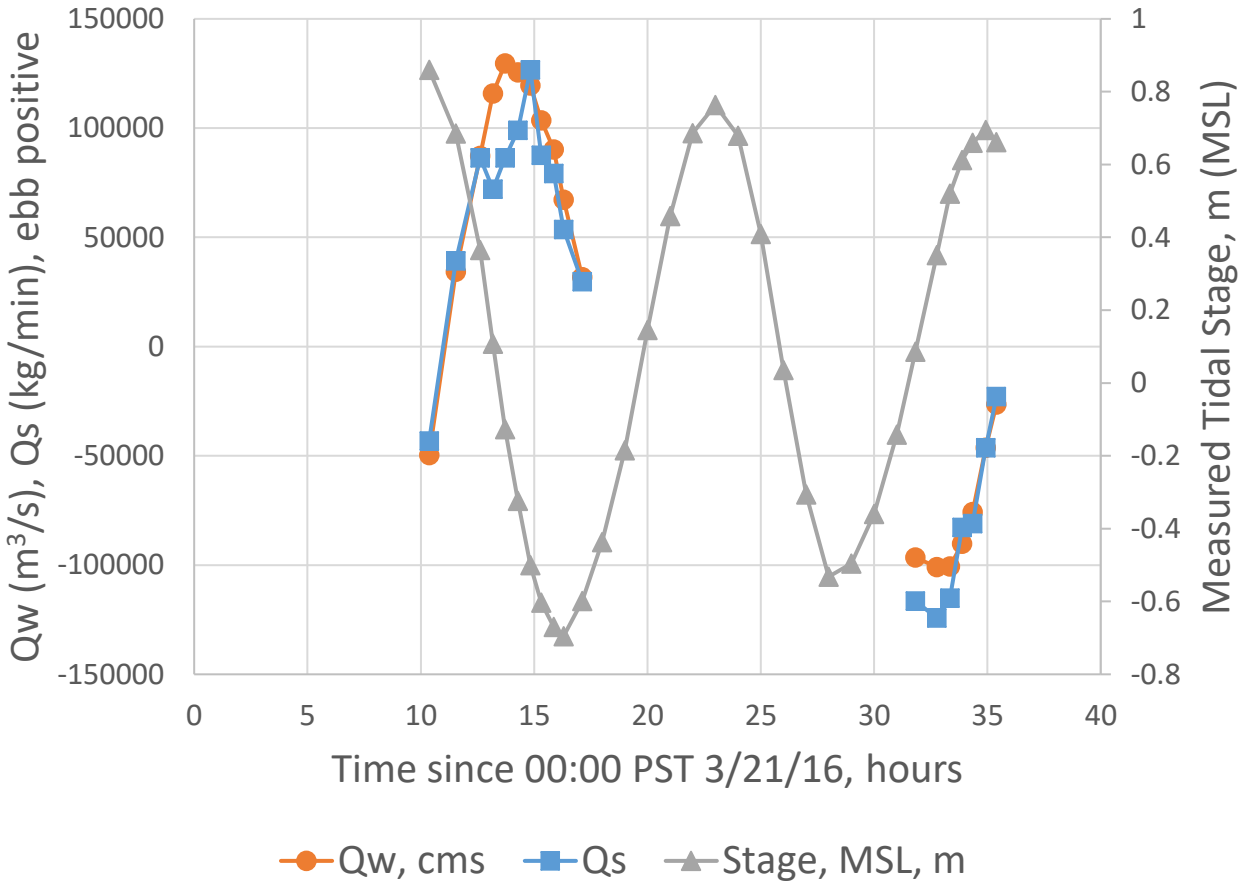

Figure 15. Time series of water flux (Qw) and suspended-sediment flux (Qs) at the Golden Gate transect for the March 2016 field campaign (see Table 3). Note Qs is reported in units of kg/min to visualize on the same scale as Qw. Positive flux indicates ebb-tide directed transport. Observed tidal stage referenced from mean sea level (MSL) is shown for San Francisco, CA NOAA station.

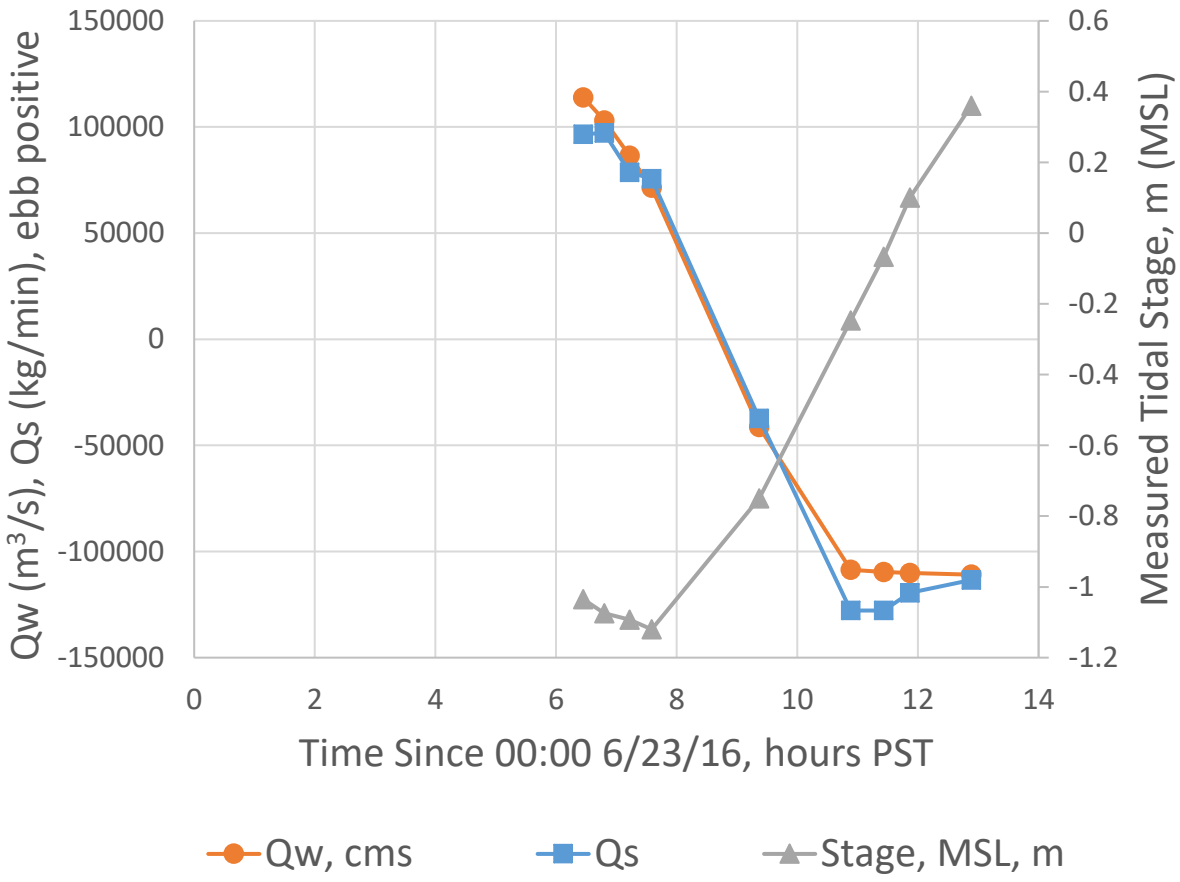

Figure 16. Time series of water flux (Qw) and suspended-sediment flux (Qs) at the Golden Gate transect for the June 2016 field campaign (see Table 4). Note Qs is reported in units of kg/min to visualize on the same scale as Qw. Positive flux indicates ebb-tide directed transport. Observed tidal stage referenced from mean sea level (MSL) is shown for San Francisco, CA NOAA station.

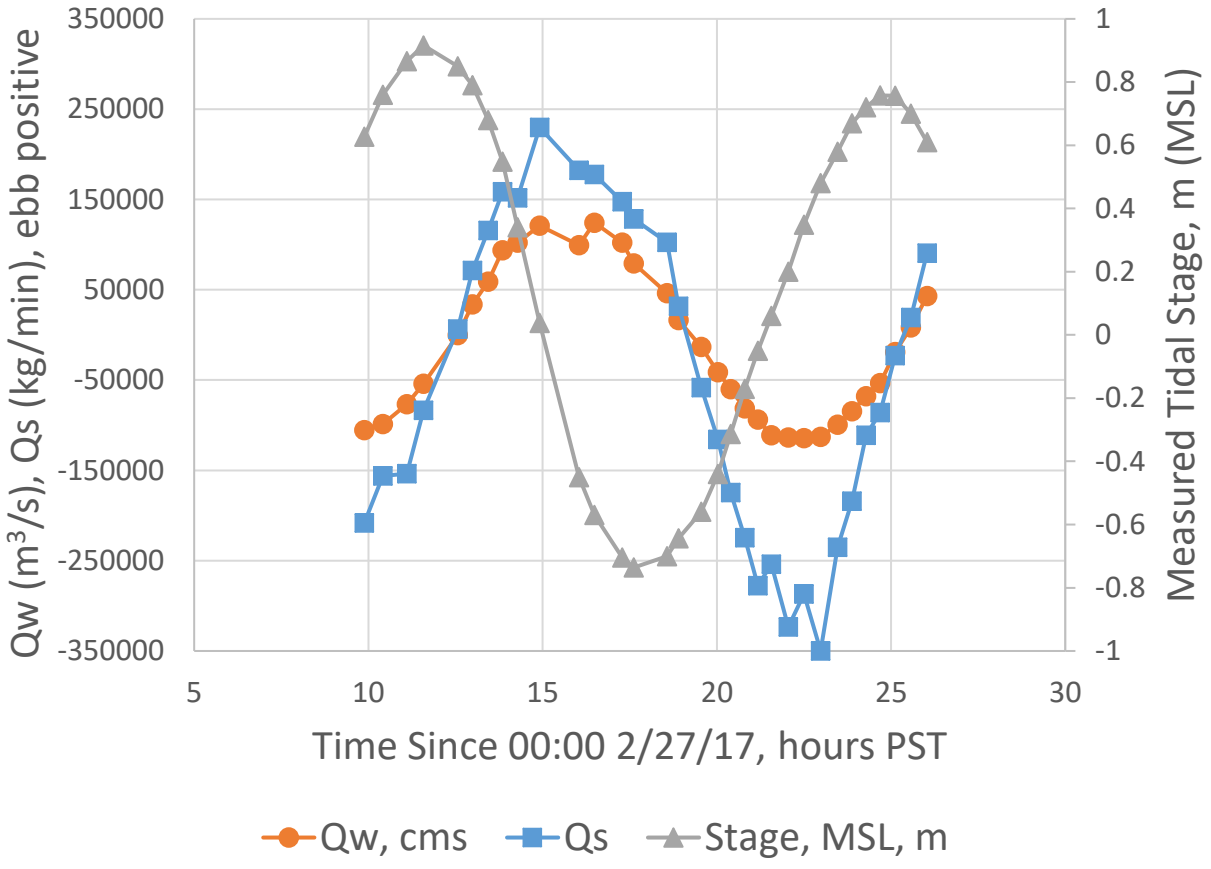

Figure 17. Time series of water flux (Qw) and suspended-sediment flux (Qs) at the Golden Gate transect for the February 2017 field campaign (see Table 5). Note Qs is reported in units of kg/min to visualize on the same scale as Qw. Positive flux indicates ebb-tide directed transport. Observed tidal stage referenced from mean sea level (MSL) is shown for San Francisco, CA NOAA station.

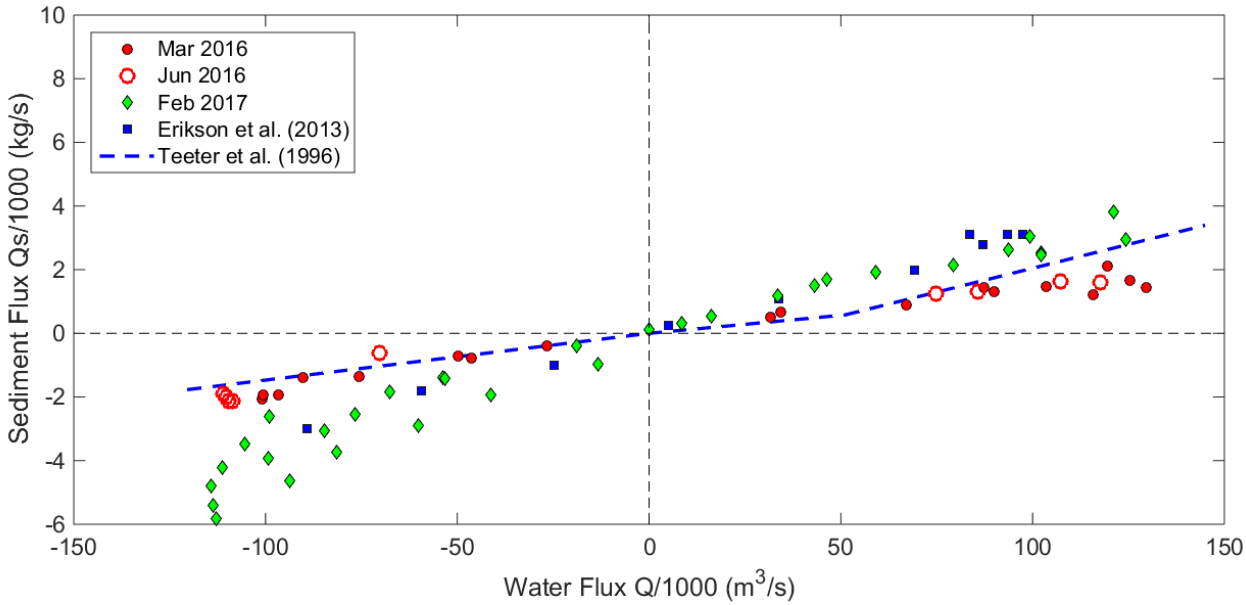

Figure 18. Scatter plot of suspended-sediment flux (Qs, y-axis) vs. water flux (Q, x-axis) for this study (Mar 2016, Jun 2016, and Feb 2017 field campaigns plotted separately) and two previous studies (Teeter et al., 1996 and Erikson et al., 2013). Values of Q and Qs were divided by 1000 to simplify axes labels. Positive values of flux indicate ebb-directed transport (out of San Francisco Bay).

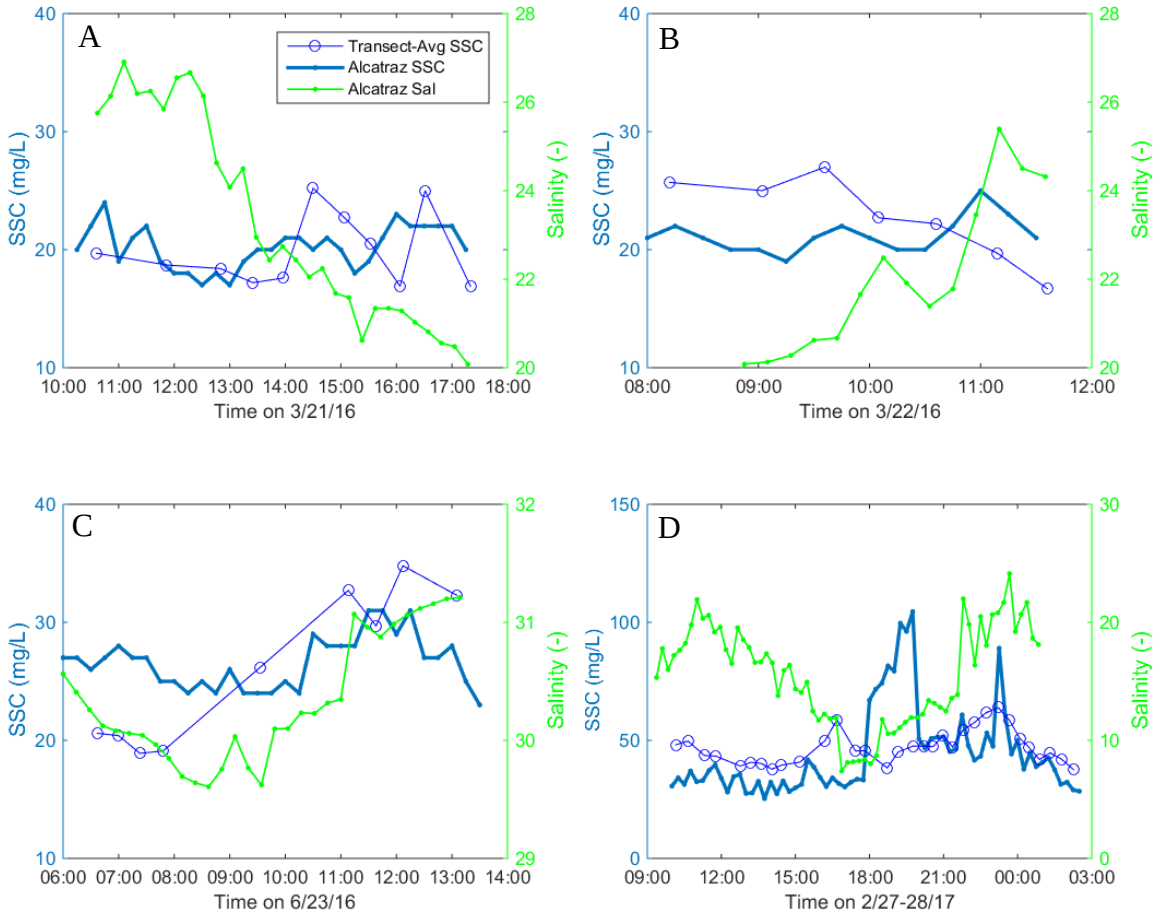

Figure 19. Time series of transect-average suspended-sediment concentration (SSC) from the Golden Gate transect and instantaneous values of SSC and salinity from the Alcatraz Island monitoring station for data collected 21 March 2016 (A), 22 March 2016 (B), 23 June 2016 (C), and 27-28 February 2017 (D). Note the different y-axis limits for SSC between A-C and D and for salinity between A-B and C and D.

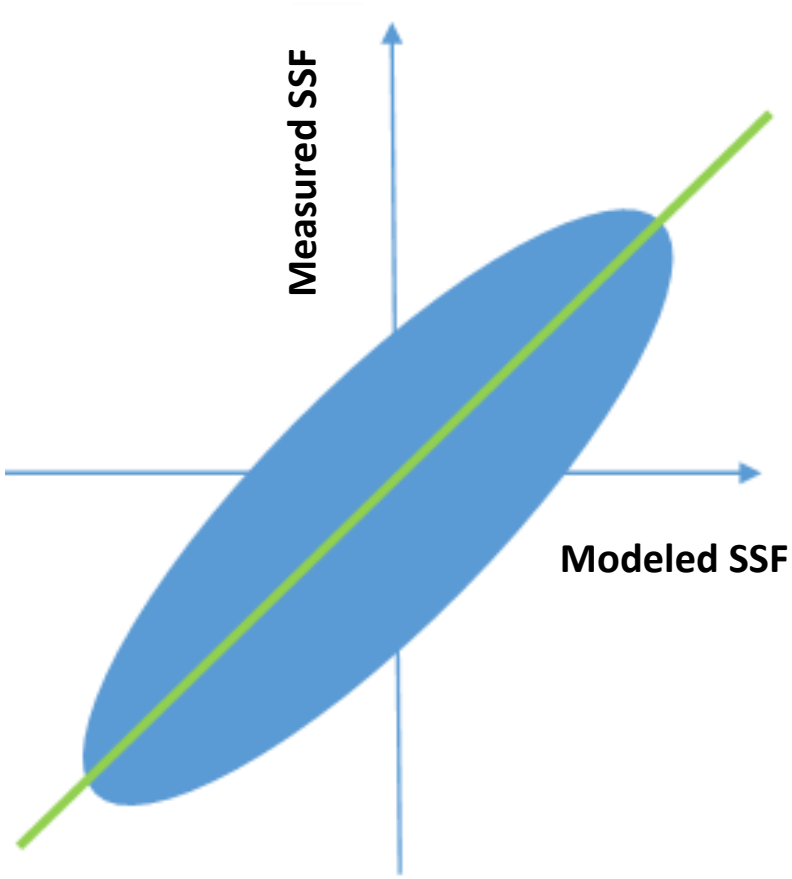

Figure 20. Hypothetical comparison of measured and modeled suspended-sediment flux (SSF). The blue ellipse represents the scatter of the data and the green line represents the best linear regression fit.